Tropical Circulation in a Time-Integration of a Global Model of the Atmosphere

SYUKURO MANABE, J. LEITH HOLLOWAY, JR., AND HUGH M. STONE

Geophysical Fluid Dynamics Laboratory, ESSA, Princeton University, N. J.

(Manuscript received 30 December 1969, in revised form 20 March 1970)

ABSTRACT

An analysis is made of the structure and energetics of the tropical circulation which emerged from a numerical time integration of a global circulation model with realistic orography.

Near the earth's surface, the general features of the time mean flow field and the location of the intertropical convergence zone of the model compare favorably with those of the actual atmosphere. Along the convergence zone or shear line, disturbances with a characteristic scale of 2000–3000 km develop and cause heavy precipitation. They tend to develop in the geographical areas where the formation of actual tropical storms is most probable. In the upper troposphere of the model tropics, disturbances with planetary scale develop and are responsible for the maximum of eddy kinetic energy there.

In general, both the kinetic energy of the tropical cyclones and that of the planetary-scale disturbances in the model tropics are chiefly maintained by the conversion of available potential energy generated by the heat of condensation. However, the planetary-scale disturbances in the upper troposphere of the tropics seem to be also affected by various factors such as the interaction with higher latitudes and land-sea contrast. It is noteworthy that these disturbances transport angular momentum across the equator in the upper troposphere and strongly affect the budget of angular momentum in the model tropics.

1. Introduction

Recently a global atmospheric circulation model with realistic orography was constructed at the Geophysical Fluid Dynamics Laboratory of ESSA. The tropical part of the model atmosphere, which emerged from the numerical time integration of the model atmosphere, has various features common to the actual tropics. For example, the general features of the time mean flow field and the location of the intertropical convergence zone compare reasonably well with those in the actual tropics. The areas of the model tropics favorable for the formation of tropical cyclones agree with the areas of frequent formation of cyclones in the actual tropics. Therefore, it was decided to perform a detailed analysis of the circulation of the model tropics. Such an analysis should be useful in speculating on how the general circulation of the actual tropics is maintained.

A similar analysis of a model atmosphere was made by Manabe and Smagorinsky (1967) and Manabe *et al.* (1965). Their model has a hemispheric domain with a free-slip insulated wall at the equator. They concluded that the kinetic energy of the disturbances in their model tropics is chiefly maintained by the release of eddy available potential energy generated by the heat of condensation. This conclusion is not inconsistent with the recent results of Riehl (1965, 1969) who analyzed the thermal structure of easterly waves and found a warm core in the upper troposphere and a cold core in the lower troposphere. He concluded that the conversion of potential energy into kinetic energy in the warm core is responsible for maintaining tropical disturbances such as easterly waves.

On the other hand, Mak (1969) constructed a theoretical model of the tropics without the effect of condensation. Based upon the results of his theoretical analysis, he concluded that the energy exchange between the tropics and higher latitudes by pressure interaction is large enough to maintain the eddy kinetic energy in the tropics. Charney (1969) also speculated that the very long waves in the upper troposphere of the tropics are produced by the energy exchange between the tropics and middle latitudes, although latent heat may be responsible for generating the disturbances in the lower tropical troposphere. In order to resolve the differences among these results, it was decided to perform numerical integrations of global circulation models with and without the effect of the condensation process. The extensive comparison among the circulations of the two model atmospheres and the actual atmosphere should be useful for identifying the cause of the difference between Mak's results and those of Manabe and Smagorinsky. Furthermore, such a comparison can be useful in determining the role of the condensation process in maintaining the general circulation of the tropics.

2. Brief description of the model

The details of the model structure are described in a companion paper which includes the general description

of the results from the time integration of the global model (Holloway and Manabe, 1970). Therefore, only a very brief sketch of the global model is given here.

The primitive equations of motion in spherical coordinates are used for this study. The effects of mountains are incorporated by use of the so-called sigma coordinate system, which identifies the earth's surface as a coordinate surface (Phillips, 1957). In order to simulate the effects of sub-grid scale mixing, a nonlinear viscosity is incorporated into the model as suggested by Smagorinsky (1963) (see Manabe *et al.*, 1970). The vertical mixing of various quantities by sub-grid scale mixing is treated in the manner described by Smagorinsky *et al.* (1965). Since the finite difference forms of the dynamical equations and the global grid system are similar to those proposed by Kurihara and Holloway (1967), they are not described here. The time integrations of the model are carried out for two different resolutions of the finite differences. The results from the low-resolution experiment are described in the main part of the text, and those from the high-resolution experiment are covered in the Appendix. (The grid sizes of the two experiments are tabulated in Table A1 of the Appendix.) In the vertical direction, nine finite difference levels are chosen so as to resolve the structure of the planetary boundary layer as well as that of the stratosphere. The approximate heights and normalized pressures of these integral levels are given in Table 1.

The scheme of computing radiative heating and cooling is identical with that described by Manabe and Strickler (1964) and Manabe and Wetherald (1967). The scheme consists of two parts, i.e., solar radiation and longwave radiation. For this study, the solar insolation of January is assumed. For the sake of simplicity the diurnal variation of solar radiation is not taken into account. The climatological distributions of water vapor, carbon dioxide, ozone and cloud cover in January are used for this computation. They are specified as a function of latitude and height.

Temperatures of continental surfaces are determined by the requirement of heat balance among the turbulent fluxes of sensible and latent heat and the net fluxes of solar and terrestrial radiation. For the sake of simplicity the ground surface is assumed to have no heat capacity. On the other hand, it is assumed that the sea surface has an infinite heat capacity. The normal distribution of sea surface temperature in February, which has been compiled by the Hydrographic Office (1944) and shown in Fig. 5.12, is used as a lower boundary condition.

The prognostic system of water vapor consists of contributions by the three-dimensional advection of water vapor, the moist convective adjustment, evaporation from the earth's surface, and condensation. This prognostic system is described in detail by Manabe *et al.* (1965). It is probably advisable, however, to describe the moist convective adjustment in some detail here for the convenience of the following discussion.

TABLE 1. Heights and normalized pressures of the levels used in the model.

Level	Normalized pressure, p/p_{surf}	Height (m)
0.5	0.00000000	∞
1.0	0.01594441	27,900
1.5	0.04334139	21,370
2.0	0.07000000	18,330
2.5	0.11305591	15,290
3.0	0.16500000	12,890
3.5	0.24081005	10,500
4.0	0.31500000	8,680
4.5	0.41204675	6,860
5.0	0.50000000	5,430
5.5	0.60672726	4,010
6.0	0.68500000	3,060
6.5	0.77337055	2,110
7.0	0.83500000	1,490
7.5	0.90154066	860
8.0	0.94000000	520
8.5	0.98010000	170
9.0	0.99000000	80
9.5	1.00000000	0

As we know, one of the most serious difficulties in designing a numerical model of the general circulation is in the parameterization of moist convection. In view of our lack of knowledge of the interaction of the small-scale convection with the large-scale fields of motion and temperature, we adopted an extremely simple system simulating the macroscopic behavior of moist convection. Despite its simplicity this system possesses at least some of the essential characteristics of the moist convection of the actual atmosphere in a qualitative sense. The basic assumptions adopted for this system of moist convection are as follows:

1) If air is saturated and the lapse rate is super-moist adiabatic, the free convection is strong enough to make the equivalent potential temperature uniform and the relative humidity everywhere saturated in the convective layer.

2) The sum of potential, internal and latent energy is conserved during the convective adjustment.

In short, moist convection neutralizes the lapse rate,[1] releases the heat of condensation, and transfers heat energy from lower layers to upper layers. It creates a cold core in the lower troposphere and a warm core in the upper troposphere. Recently, Riehl (1969) found a similar thermal structure in the moist convective regions of easterly waves. In this study we attempt to show how the circulation of the model tropics responds to this idealized convective adjustment. This type of investigation may yield information on how one can further improve the parameterization of moist convection.

[1] By neutralizing the lapse rate the moist convective adjustment prevents the so-called convective instability of the first kind which usually results from unstable stratification and causes grid-scale convection in the model atmosphere.

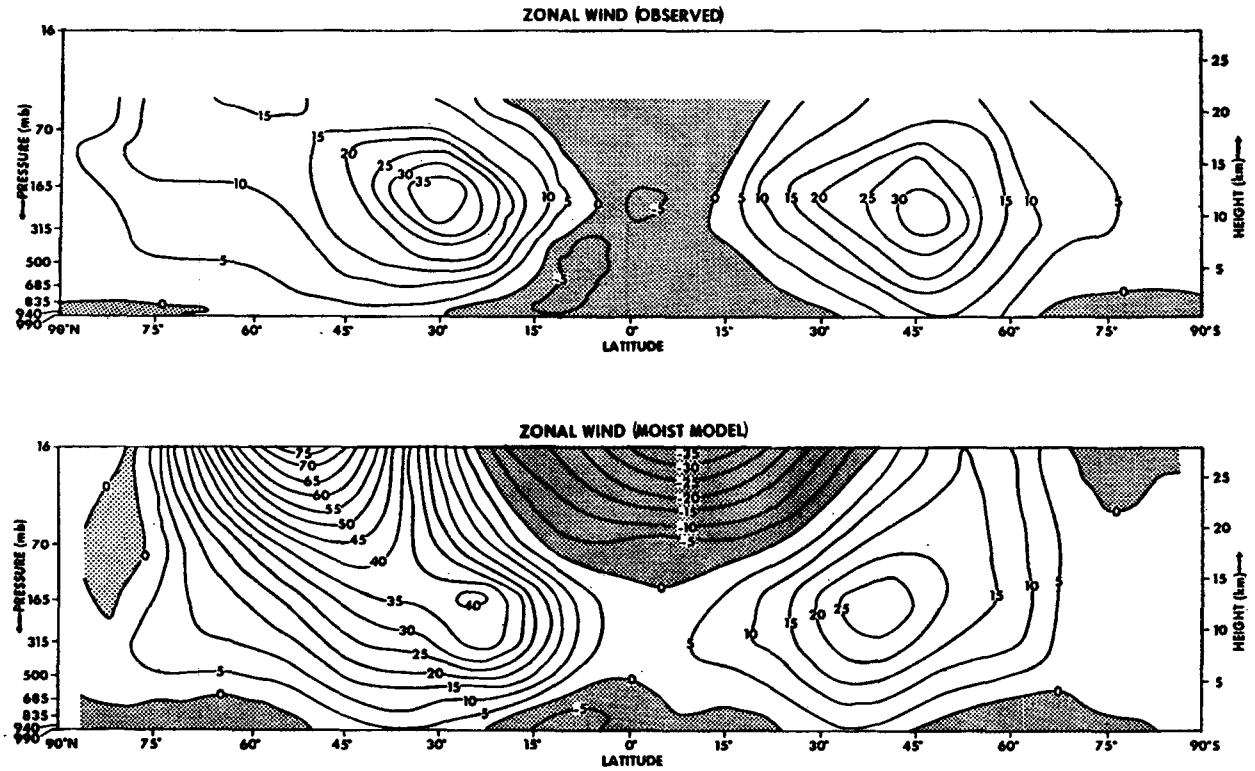

FIG. 3.1. Latitude-height distribution of the zonal mean of the zonal wind (m sec^{-1}): upper part, observed [Northern Hemisphere (Oort and Rasmusson, 1970b), Southern Hemisphere (van Loon *et al.*, 1969)]; lower part, moist model atmosphere.

The schemes for computing the hydrology of the ground surface are very similar to those described by Manabe (1969). The rates of the change of soil moisture and snow depth are based upon the budget requirements of water, snow and heat. It is important to note that snow cover has a very large effect upon the heat balance of the earth's surface by markedly increasing the albedo of the ground surface.

The numerical time integration was continued until the model atmosphere reached the state of so-called "quasi-equilibrium." As mentioned in the introduction, we performed two integrations of the global model—with and without the selective heating by condensation—in order to isolate the role of the condensation process in maintaining the general circulation of the atmosphere. Hereafter, the model with a prognostic system for water vapor will be called "the moist model" and the model without it will be called "the dry model." It must be pointed out, however, that the dry model does have a process of simple moist convective adjustment of its static stability to prevent the lapse rate from becoming moist-adiabatically unstable. In the dry model, convection can occur in any moist-adiabatically unstable layer; whereas in the moist model, it is necessary for the air to be saturated in order for condensation and moist convection to take place. Further detail concerning the structure of the dry model may be found in the paper by Smagorinsky *et al.* (1965). A time integration of a model very similar to the dry model described here has already been carried out by Mintz and Arakawa (see Mintz, 1965).

The initial condition for the numerical time integration of the moist model is a zonal mean state which was obtained from the integration of the hemispheric model (Manabe *et al.*, 1965). The period of the integration of the moist model was 341 days; toward the end of this period the atmosphere had essentially reached the quasi-equilibrium state.

For the dry model, the state of the moist atmosphere on the 279th day of the time integration was used as an initial condition. The period of the time integration of the dry model was 96 days.

3. Time mean fields

The distributions of various quantities which are shown in this section represent averages over a certain period of time. The averaging period for the moist atmosphere was a 40-day period starting from the 302nd day of the moist model integration and that for the dry atmosphere a 40-day period starting from the 56th day of the dry model integration.

Fig. 3.1 shows the latitude-height distributions of the zonal mean of zonal wind in the moist model atmosphere and in the actual atmosphere of January. In the lower troposphere of the model tropics, the region of the

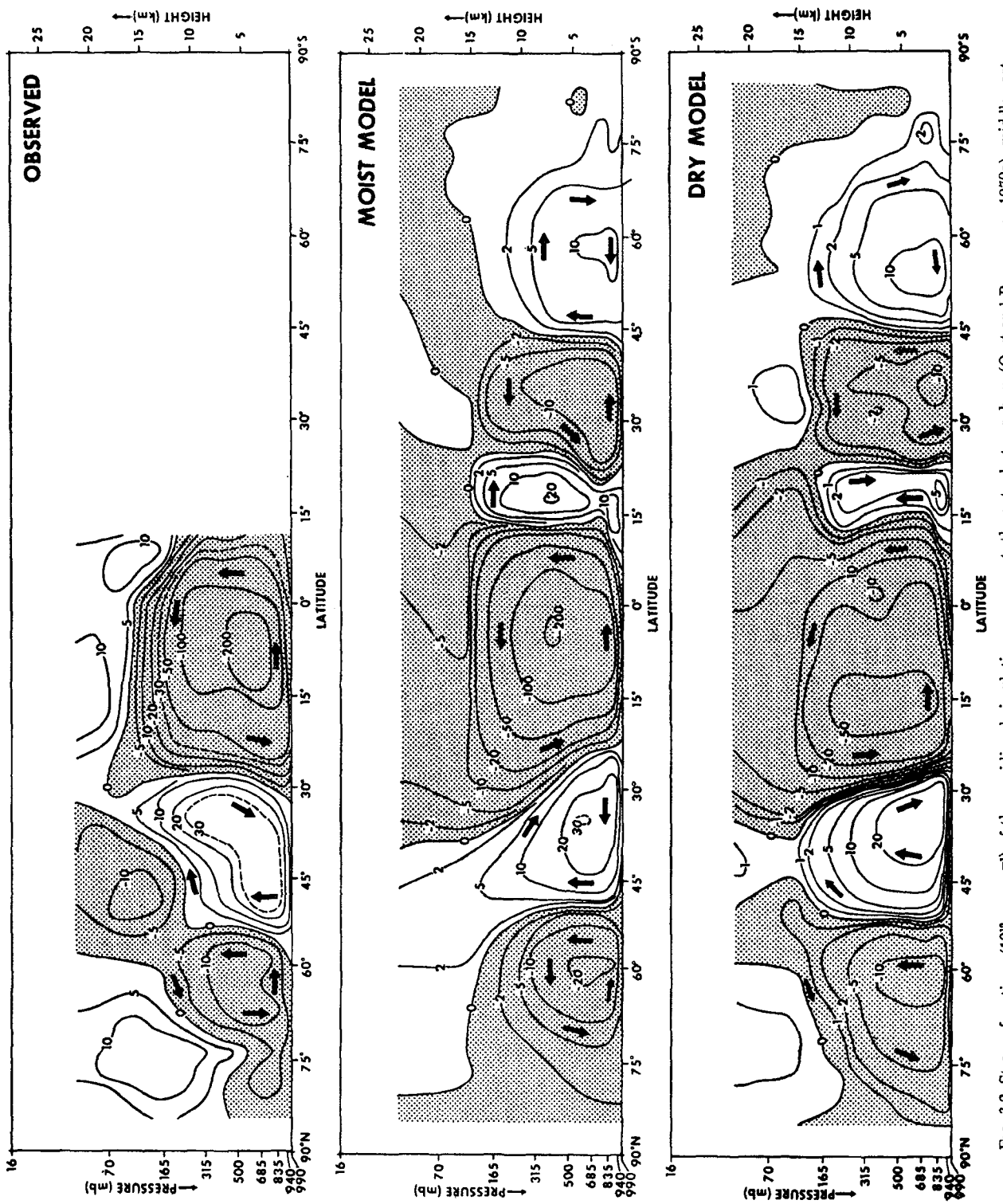

FIG. 3.2. Stream functions (10^{12} gm sec^{-1}) of the meridional circulation: upper part, the actual atmosphere (Oort and Rasmusson, 1970a); middle part, moist model; lower part, dry model. Note that contours are drawn in logarithmic intervals.

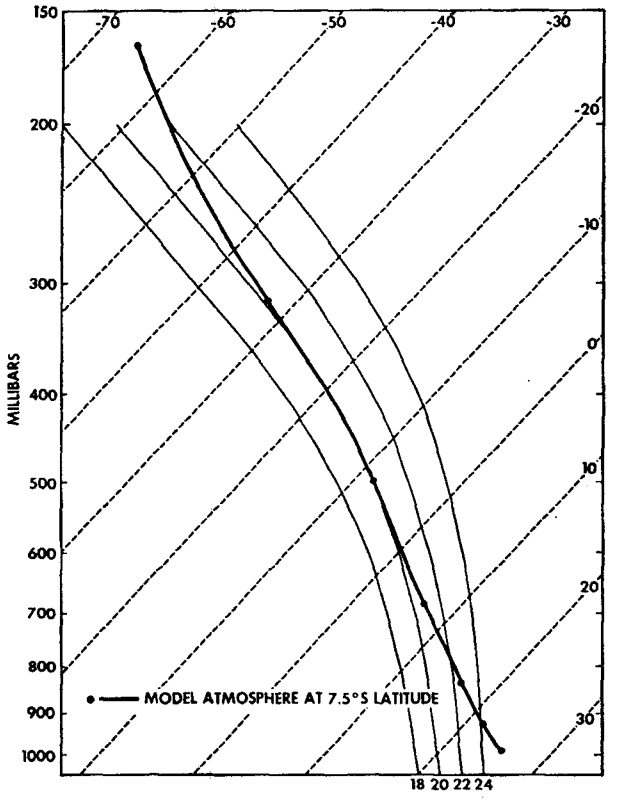

FIG. 3.3. Vertical distribution of zonal mean temperature at 7.5S latitude of the moist model. Slanted dashed lines are isotherms. Thin solid lines are moist adiabats.

easterly wind is maintained in agreement with that feature of the actual tropics. A weak westerly, however, appears in the upper troposphere where the actual tropics maintains an easterly. The cause of this discrepancy is not obvious, although it will be shown in the Appendix that weak tropical westerlies disappear as a result of the increase in the horizontal resolution of the finite differences of the model. In the stratosphere of the model tropics, an intense easterly predominates. It is much more intense than the actual easterly which can be identified in the upper half of Fig. 3.1. Such a strong easterly is observed only during limited periods of time in the actual stratosphere. [See, for example, the paper by Reed (1962) which describes the biennial oscillation of zonal currents in the tropical stratosphere.] Preliminary results from the time integration of a global model incorporating a seasonal variation of solar radiation show a markedly reduced intensity of the easterlies in the stratosphere of the model tropics. Therefore, it is probable that the intense easterlies in the model stratosphere result from the assumption of a perpetual January.

The stream function of the meridional circulation in the moist atmosphere is shown in the middle part of Fig. 3.2. According to this figure, an intense direct Hadley cell predominates in the model tropics. The upward branch of the cell is located between the equator and 10S. The intensity of this cell is approximately 200×10^{12} gm sec^{-1}, whereas that of the Hadley cell in the Southern Hemisphere is very weak. This difference in the intensities of the two Hadley cells is obviously caused by the asymmetry between the boundary conditions of the two hemispheres. In general, these features of the Hadley cells in the model atmosphere are in excellent agreement with those of the Hadley cells in the actual tropics shown in the upper part of Fig. 3.2. The stream function of the meridional circulation in the actual atmosphere in January was computed by Oort and Rasmusson (1970a) from data tapes of the MIT general calculation library covering a period of five years. Previously, Kidson *et al.* (1969) obtained Hadley cells with similar features in their study of the general circulation of the tropics.

In their study of the tropical circulation of a hemispheric model, Manabe and Smagorinsky (1967) concluded that the condensation process markedly increases the intensity of the Hadley cell. In order to confirm their conclusion the stream function of the meridional circulation in the dry model atmosphere is shown in the lower part of Fig. 3.2. A comparison between the intensities of the Hadley cell in the dry and moist model atmospheres indicates that the heat of condensation intensifies the Hadley cell of the global model by a factor of as much as 4. It must be pointed out also that the intensity of the weak Hadley cell in the Southern Hemisphere also increased as a result of the incorporation of the effect of condensation.

The vertical distribution of temperature in the model tropics is shown in Fig. 3.3. For reference, curves indicating atmospheres with moist adiabatic lapse rates are added to the same figure. According to this figure, the static stability of the model tropics is super-moist adiabatic below the 400-mb level and is sub-moist adiabatic above this level. A similar result was obtained by Manabe and Smagorinsky (1967). As demonstrated in the following sections, this vertical distribution of temperature has a profound effect on the energetics of tropical disturbances.

The distribution of the wind field near the earth's surface is shown in Fig. 3.4. In the upper part of this figure the streamline map of the actual atmosphere of January constructed by Mintz and Dean (1952) is shown. In the middle part of this figure, the time-mean streamline map of the moist model atmosphere at the 940-mb level is presented. In general, the locations of the intertropical convergence zones of the moist model agree well with those in the actual atmosphere. Furthermore, the angle of confluence into the convergence zones of the model is highly realistic. Detailed examination of the results, however, reveals that the intertropical convergence zone in the eastern Pacific of the model is located too close to the equator, probably as a result of inaccuracy in the distribution of sea-surface temperatures chosen for this study. As Fig. 5.12 indicates, the distribution of the sea-surface temperature in the

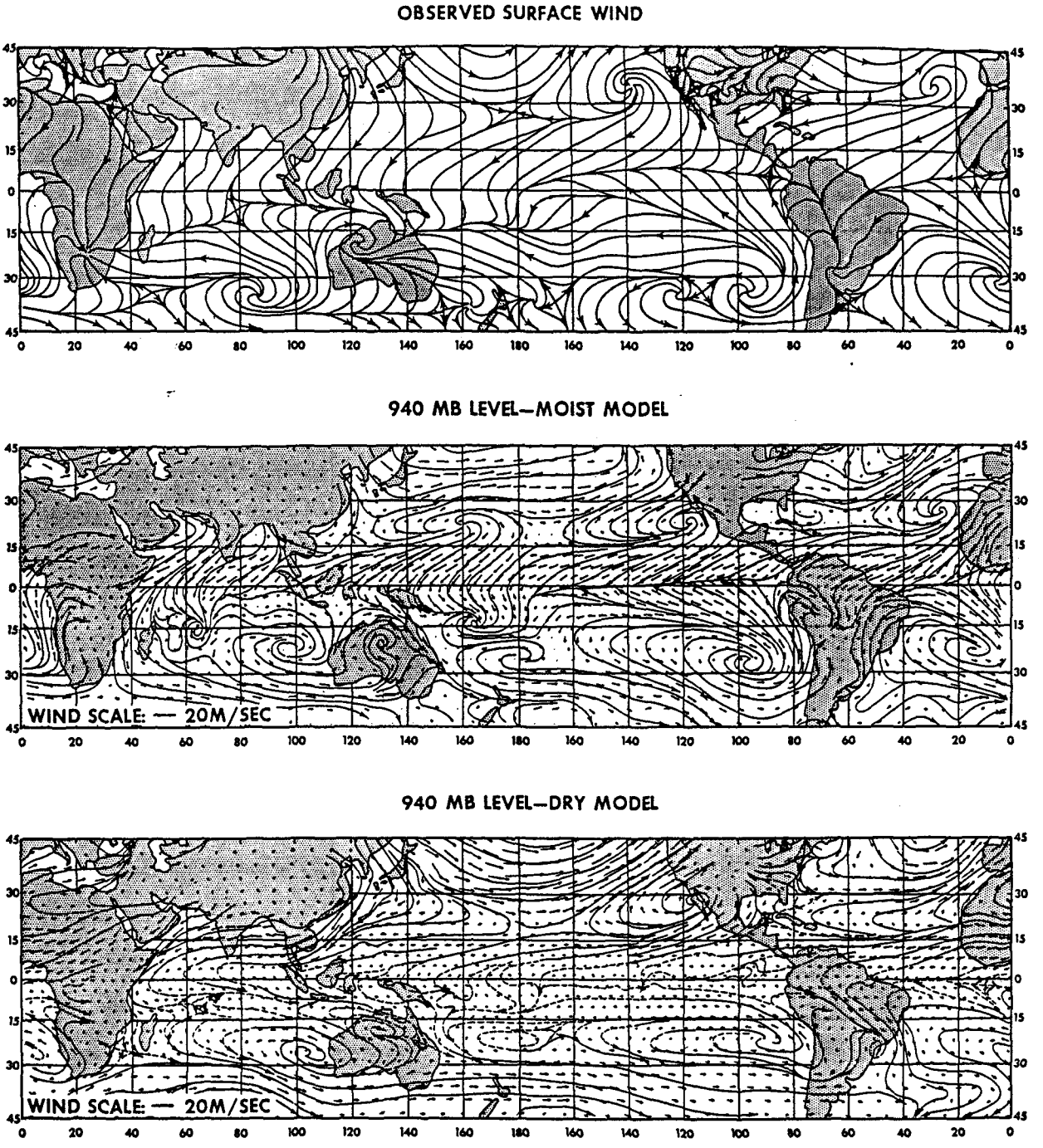

FIG. 3.4. Time-mean maps of wind vectors and streamlines near the earth's surface: upper part, streamlines at the earth's surface (Mintz and Dean, 1952); middle part, the moist atmosphere; lower part, the dry atmosphere.

eastern Pacific of the model is somewhat different from the distribution recently published by the Hydrographic Office (1969), i.e., it lacks the zone of distinct minimum temperature along the equator which is evident in the new version. As discussed by Manabe (1969), relatively low sea-surface temperatures tend to prevent the genesis of tropical disturbances and accordingly lower the rate of precipitation. Therefore, the intertropical convergence zone does not usually coincide with an area of low sea-surface temperature. It is highly probable that the intertropical convergence zone in the eastern Pacific of the model would have been located to the north of the equator had we used the new version of the sea-surface temperatures. Another feature of interest in the time-mean map is the appearance of cyclonic vortices located to the east of New Guinea and to the east of Madagascar.

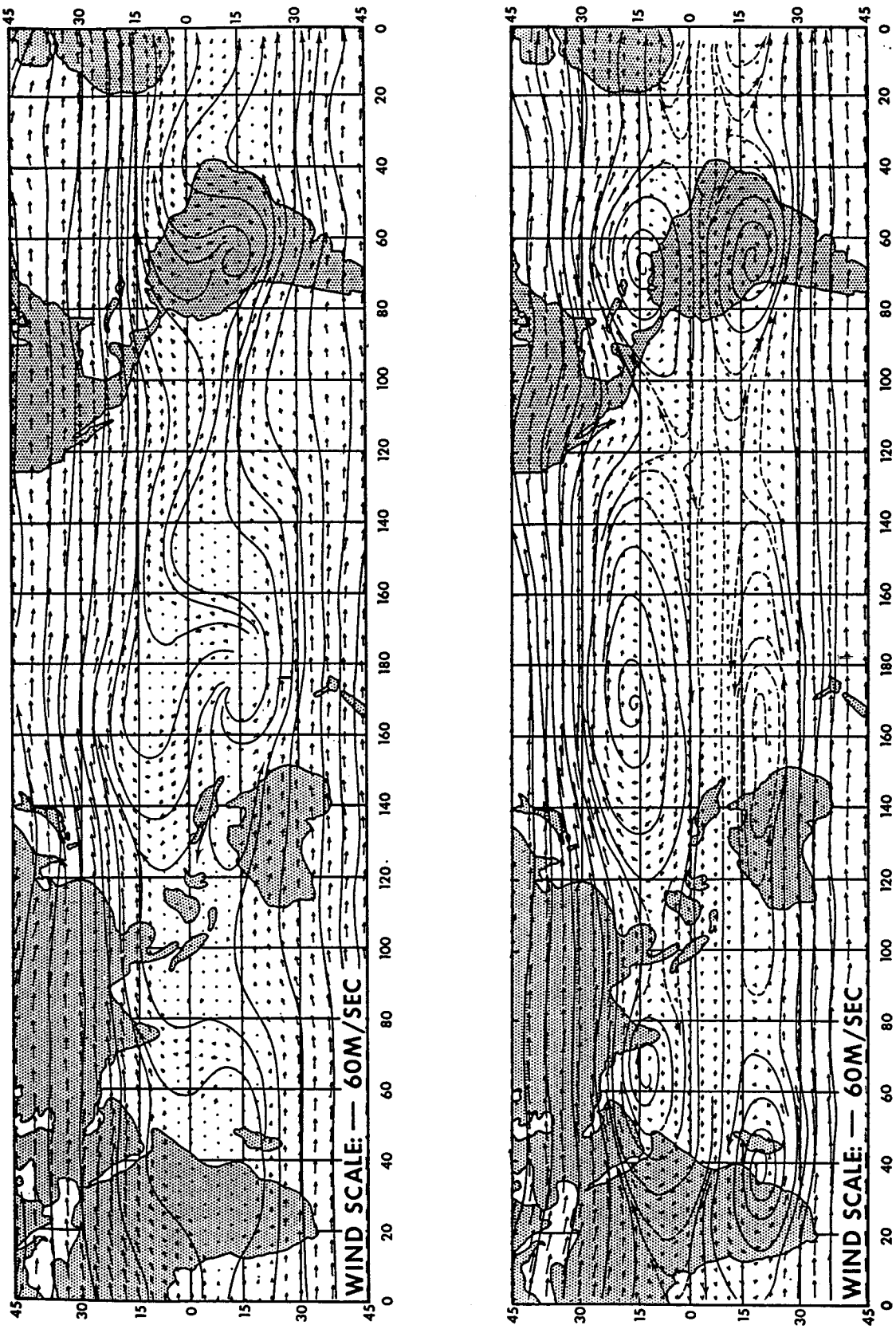

FIG. 3.5. Time-mean maps of wind vectors and streamlines at the 165-mb level: upper half, the moist model; lower half, the dry model.

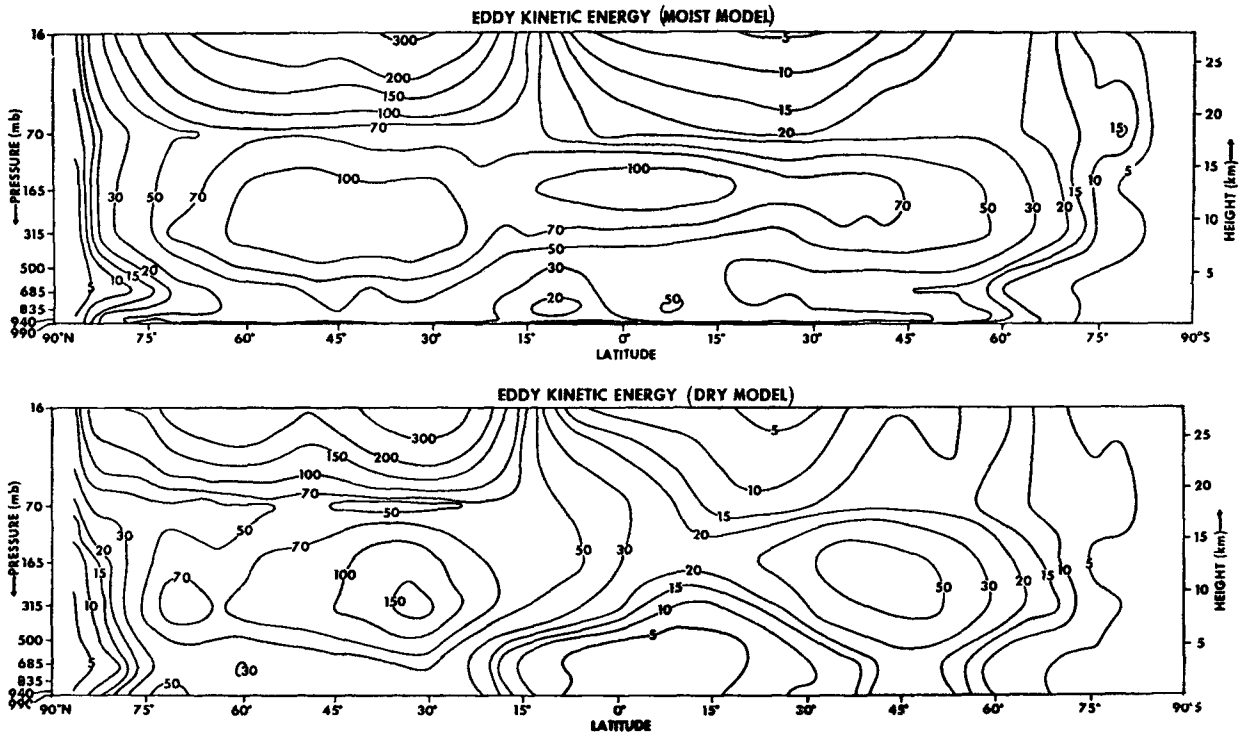

FIG. 4.1. Latitude-height distribution of eddy kinetic energy (10^{-3} J cm^{-2} mb^{-1}): upper half, the moist model; lower half, the dry model.

These are the areas where it is most probable for a tropical cyclone to form during January and February. In Section 5, we shall discuss the formation and the development of tropical cyclones in these areas of the model tropics.

In the subtropics of the model, there are many oceanic anticyclones. As Fig. 3.4 indicates, air masses which flow out of these anticyclones converge into the intertropical convergence zones. Although these anticyclones are located too close to the equator by several degrees,[2] it is usually possible to find their counterparts in the actual atmosphere.

The influence of the condensation process on the flow field near the surface of the model earth is evident if one compares the flow field of the moist model with that of the dry model shown in the lower part of Fig. 3.4. The intertropical convergence of the dry model is much weaker than that of the moist model and is barely detectable. The location of the convergence zone, however, agrees approximately with that of the moist model. This result seems to indicate that the location of the intertropical convergence zone is mainly controlled by the processes incorporated into the dry model, although the remarkable intensification of the intertropical convergence by the heat of condensation makes the flow field of the moist tropics much more realistic than that of the dry tropics. A similar comparison between the flow field in the upper troposphere of the moist model and the flow in the dry model is made in Fig. 3.5. In the upper troposphere of the moist model, intense divergence takes place over three major rainfall areas, i.e., the western part of the Indian Ocean, the Southwest Pacific, and the northern plains of South America. S-shaped cross-equatorial currents of significant intensity originate from these areas and account for most of the poleward mass transport of the Hadley cell in the upper troposphere of the moist model tropics. A recent analysis of satellite pictures by Johnson (1969) indicates the existence of such cross-equatorial currents. In the upper troposphere of the dry model atmosphere, such cross-equatorial currents are small and are not evident. However, the locations of anticyclonic vortices in the Southern Hemisphere of the dry model correspond very well with the source regions of three major cross-equatorial currents in the moist model atmosphere. Again, these results seem to indicate that the locations of the cross-equatorial currents are essentially controlled by the processes incorporated into the dry model, although the currents are mostly driven by the heat of condensation. It is not clear, however, whether the locations of the currents are mainly controlled by the interaction with higher latitudes or the influences from the lower boundary.

4. Eddy kinetic energy

The latitude-height distribution of eddy kinetic energy in the moist model atmosphere is shown in the upper half of Fig. 4.1. According to this figure, the eddy

[2] The latitudes of the anticyclones are closer to realistic values in the results of the high-resolution model described in the Appendix.

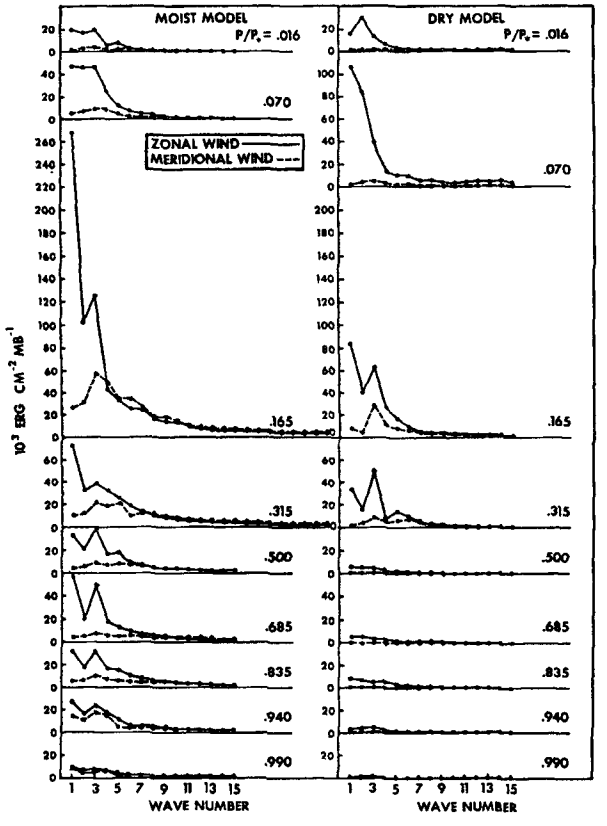

FIG. 4.2. Spectra of eddy kinetic energy of zonal and meridional components of the wind at various levels in the model tropics (11.25N–11.25S): left-hand side, the moist model; right-hand side, the dry model.

kinetic energy in the model tropics is a maximum just below the tropical tropopause in agreement with the features of the actual atmosphere [see, for example, Oort and Rasmusson (1970b)]. This maximum value, however, is as large as the eddy kinetic energy in middle latitudes of the moist model. In the actual atmosphere, the eddy kinetic energy in middle latitudes is much larger than that in the tropics. This unrealistic feature of the moist atmosphere disappears as a result of the doubling of the resolution of horizontal finite differences. As is shown in the Appendix (sub-section b), the doubling of the resolution markedly increases the eddy kinetic energy in middle latitudes, whereas it changes little the maximum value in the moist model tropics.

In the lower troposphere of the moist model tropics, a region of secondary maximum is evident to the south of the equator indicating the predominance of disturbances in this region. It is well known that tropical cyclones usually form to the south of the equator during January or February. Such cyclones may be responsible for the secondary maximum of eddy kinetic energy mentioned above. We shall discuss the statistics of the formation and the development of tropical cyclones in the next section.

According to the comparison between the distributions of eddy kinetic energy in the moist and dry tropics which are shown in Fig. 4.1, the heat of condensation markedly increases the eddy kinetic energy in the model tropics particularly in the upper troposphere. In the Appendix, it is shown that the distribution of eddy kinetic energy in the tropics of the high-resolution moist model compares very favorably with that in the actual tropics.

The spectra of eddy kinetic energy at various levels of the tropics of the moist model are shown in the left-hand side of Fig. 4.2. As can be seen, very long waves predominate in the upper troposphere. Particularly, the eddy kinetic energy of the zonal component is very large in the range of wavenumbers 1–3. The eddy kinetic energy of the meridional component attains a maximum value at wavenumber 3. As Fig. 3.5 indicates, the time mean flow field in the upper troposphere of the moist model tropics exhibits a planetary-scale pattern with wavenumber of $\sim$3, which may be partially responsible for this maximum. In the lower troposphere the eddy kinetic energy is again relatively large at low wavenumbers. The energy spectrum, however, has a long tail toward high wavenumbers, indicating the prevalence of small-scale disturbances.

In the right-hand side of Fig. 4.2, spectra of the eddy kinetic energy in the dry model tropics are shown. Again, very long waves predominate in the upper troposphere. The shape of the spectrum is very similar to that in the upper troposphere of the moist tropics although the amplitude is quite different. For example, the spectrum of the meridional component at the 165-mb level has a maximum at wavenumber 3; and the spectrum of the zonal component at the same level has a maximum at wavenumber 1, a secondary maximum at wavenumber 3, and generally decreases with increasing wavenumber in both the moist and the dry atmospheres. The similarity between the two spectra seems to indicate that the characteristic scale of disturbances with planetary scale is, in part, controlled by factors incorporated into the dry model. On the other hand, the moist processes markedly increase the amplitude of these disturbances. In the lower troposphere of the dry model, the magnitudes of the eddy kinetic energy spectral components are practically zero. This result seems to suggest that the condensation process is indispensable for the maintainance of the eddy kinetic energy in the lower troposphere of the moist model tropics.

5. Structure of the tropical disturbances

In order to give a general idea of the characteristic features of the flow field in the moist model tropics, streamline maps on two isobaric levels on the 307th day of the time integration of the moist model are shown in Fig. 5.1. At the 165-mb level, the flow field is character-

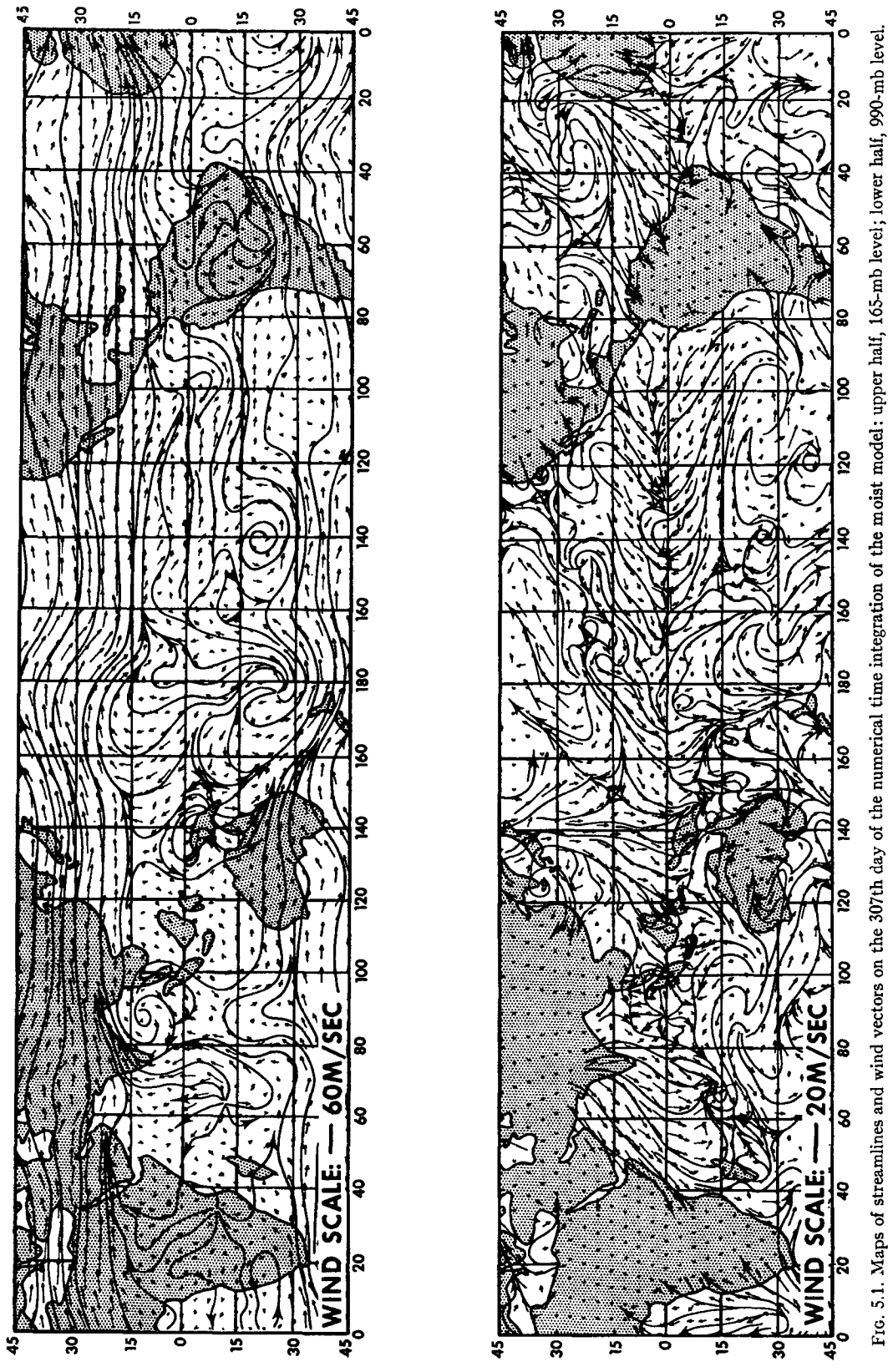

FIG. 5.1. Maps of streamlines and wind vectors on the 307th day of the numerical time integration of the moist model: upper half, 165-mb level; lower half, 990-mb level.

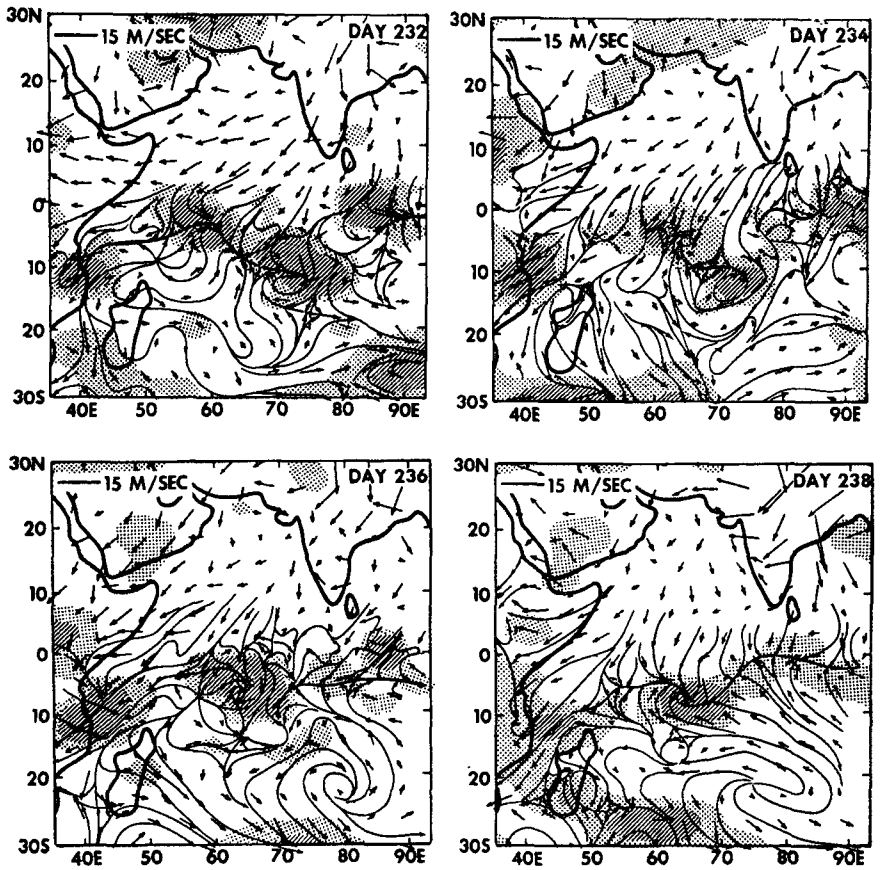

FIG. 5.2a. Maps of streamlines and wind vectors in the general area of the Indian Ocean on alternate days of the period from the 232nd to the 238th day, inclusive. The checkered shading indicates areas where daily rainfall ≥ 10 cm; slashed shading, where daily rainfall ≥ 1 cm, but <10 cm; and dotted shading indicates areas where the daily rainfall >0.1 cm, but <1 cm.

ized by interhemispheric flow and centers of strong divergence coupled with low-level convergence. Such an interhemispheric flow is also evident in Fig. 3.5 which shows the time-mean flow field.

One of the most typical features of the flow field at the 990-mb level, which is shown in the lower half of Fig. 5.1, is the development of lines of intense convergence or shear lines. Easterly winds with a significant equatorward component blow from both hemispheres and collide at the shear line. In the Indian Ocean, one can see a small cyclonic vortex on the shear line located to the south of the equator. Such a localized disturbance forms frequently in selected areas of the tropics and reminds us of storms in the actual tropics. Therefore, it was decided to perform a detailed analysis of an example of such a tropical cyclone which emerged from the integration of the global moist model.

On the 232nd model day, a tropical disturbance formed in the western part of the Indian Ocean. Figs. 5.2a and 5.2b show a series of the maps of the streamlines which trace the development of this tropical disturbance. Shading indicating 24-hr rainfall is superimposed on these maps. In addition, a series of surface pressure maps covering the same period is shown in Fig. 5.3. According to these figures, a vortex accompanied by heavy precipitation is first visible along the shear line at about 5S in the streamline map of day 234. The vortex remains nearly stationary until the pressure depression becomes evident on day 238. The streamline map indicates strong convergence of air near the earth's surface. On the other hand, the streamline map of the upper troposphere shown in Fig. 5.3a reveals strong divergence from the center of the vortex. After the formation of the depression, the cyclone then moves nearly straight southward for the next 10 days. Pressure drops gradually to a low of 981 mb on day 246; then it begins rising. The cyclone gradually transforms into an extratropical cyclone and moves off the map on day 248. Fig. 5.4 shows a time series of minimum surface pressure, maximum surface wind, and maximum rainfall, which accompany this disturbance.

In order to determine the structure of the cyclone described above, the features of the cyclone on day 246 are analyzed along the straight line shown in Fig. 5.2b. Day 246 is chosen because the cyclone is then at about the stage of maximum development. Fig. 5.5 indicates

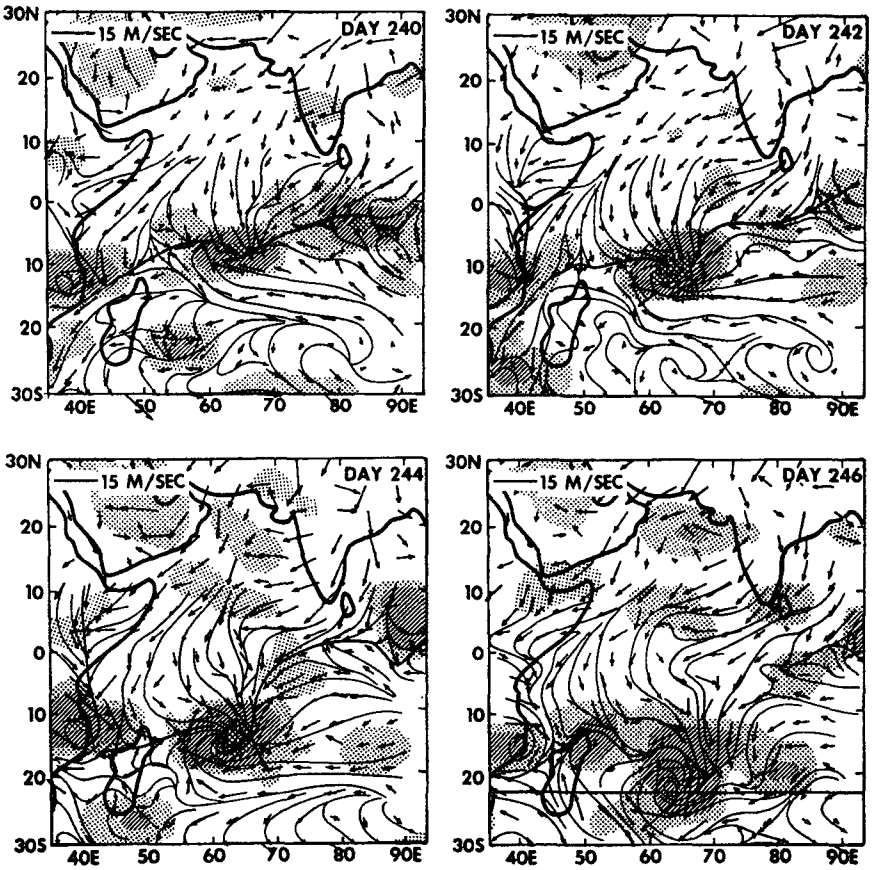

FIG. 5.2b. Continuation of Fig. 5.2a for the period from the 240th to the 246th day inclusive.

the distribution of the deviation of pressure from the zonal mean on this cross section. According to this figure, a low pressure anomaly occupies most of the troposphere. A weak high pressure anomaly, however, appears above the 300-mb level. If one contrasts the distribution of pressure anomaly with those of relative humidity and vertical motion, which are shown in Figs. 5.6 and 5.7, respectively, one notes that a humid tower is maintained at the center of the tropical cyclone where upward motion predominates. As Fig. 5.8 indicates, the vertical distribution of temperature in this humid tower has a moist adiabatic lapse rate revealing that the moist convective adjustment is executed in the tower. This distribution of temperature in the humid tower may be compared with that of the zonal mean temperature of the model tropics, which is added to the same figure. According to this comparison, the humid tower has a warm core above the 800-mb level and a cold core below this level. As described in Section 3, the static stability is super-moist adiabatic below the 400-mb level and is sub-moist adiabatic above this level. Therefore, the warm core is most pronounced at about the 400-mb level. Similar features are evident in Fig. 5.9 which shows the distribution of the temperature deviation from the zonal mean along the cross section. Since the vertical motion is strongest in the upper troposphere, it is clear that eddy available potential energy is released in this humid tower.

Fig. 5.9 indicates that the thermal structure of the cyclone is not resolved sufficiently by the finite difference grid. (The pip marks at the bottom of the figure indicate the location of grid points.) Therefore, further increase in the resolution of the horizontal finite differencing is necessary in order to make sure that the vortex is not the consequence of truncation error of the numerical computation. In the Appendix (sub-section d), it is shown that the structure of the cyclone is resolved better by a finer grid system.

Fig. 5.10 shows the life history of the humid tower, i.e., the time change of the vertical distribution of relative humidity, temperature anomaly, and vertical motion. According to this figure, the humid tower grows very rapidly from day 234 to day 235 and extends throughout the troposphere[3] after day 235. During the period from day 235 to 247, the warm anomaly extends

[3] The solenoidal field resulting from the local warm anomaly over the ocean surface initiates the local upward motion and produces the humid layer which satisfies the condition for convective adjustment. As we explained in Section 2, the convective adjustment creates a warm anomaly at a higher level (and a cold anomaly below). The solenoidal field resulting from this new warm anomaly again induces more upward motion. Thus, the humid tower rapidly extends upward.

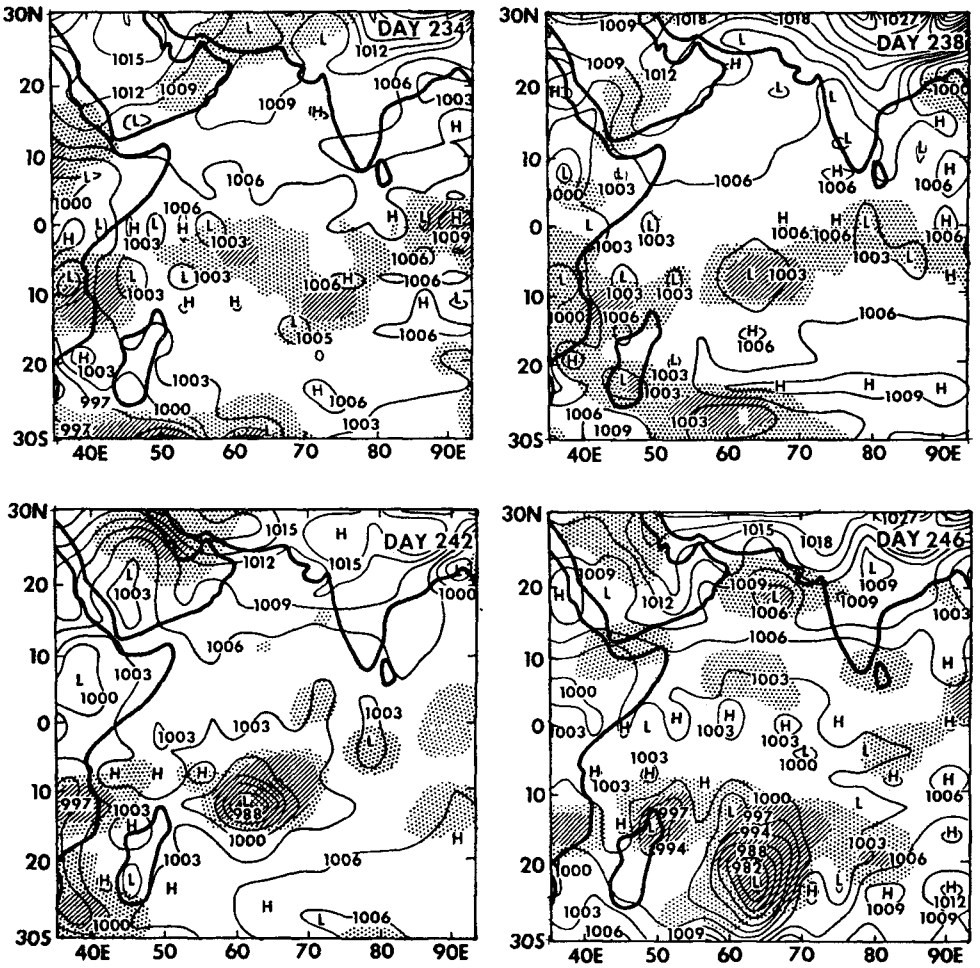

FIG. 5.3. Maps of surface pressure (mb) in the general area of the Indian Ocean. Precipitation is shaded the same as in Fig. 5.2a. Alternating series of small highs and lows along the equator indicate the appearance of the computation made.

gradually from the upper troposphere downward, whereas the magnitude of the cold anomaly slowly

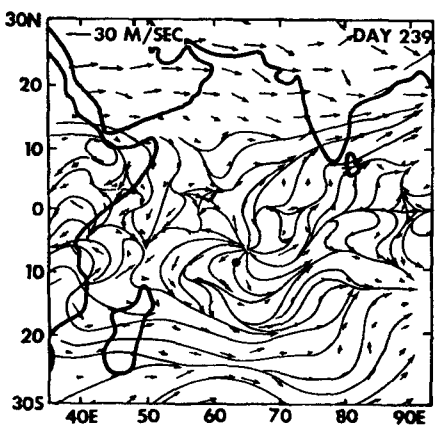

FIG. 5.3a. Streamline map of the 165-mb level above a tropical cyclone on day 239. The position of the surface cyclone is indicated by a large dot.

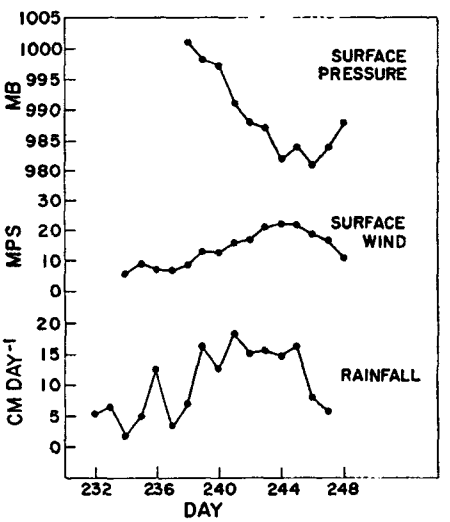

FIG. 5.4. The time series of minimum surface pressure, maximum surface wind, and maximum rainfall at the grid point closest to the center of the tropical cyclone shown in Figs. 5.2a and 5.2b.

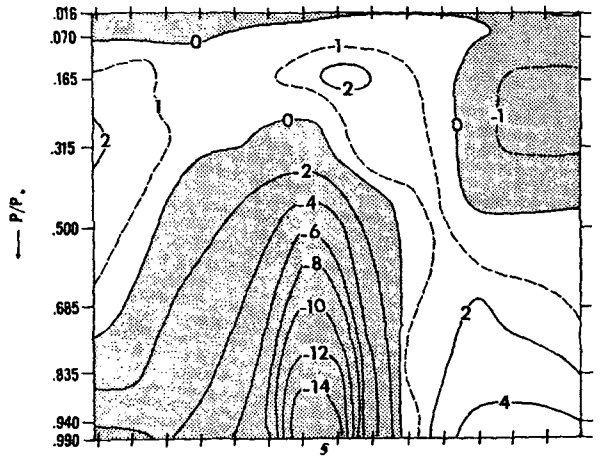

FIG. 5.5. The deviation of pressure (mb) from the zonal mean on the 246th day along the cross section indicated by the solid line in Fig. 5.2b. Pip marks at the bottom of the figure indicate the locations of grid points.

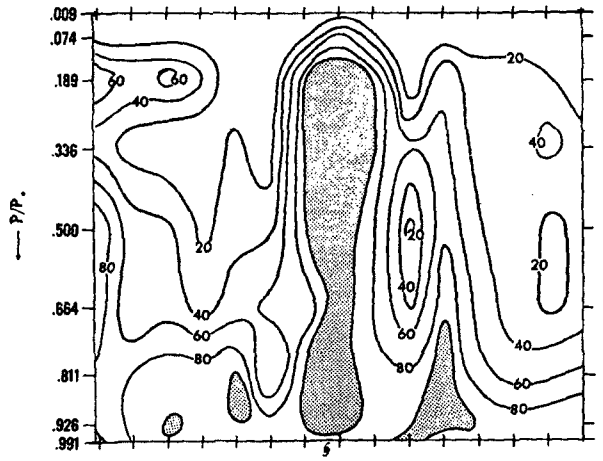

FIG. 5.6. The distribution of relative humidity on the 246th day along the cross section indicated by solid line in Fig. 5.2b. Shading indicates regions of saturation.

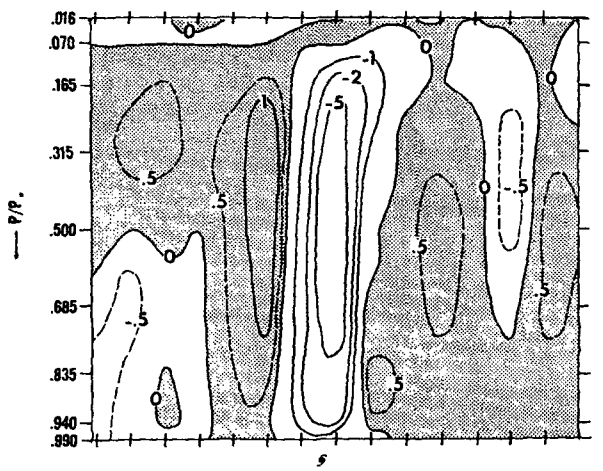

FIG. 5.7. The distribution of vertical p velocity on the 246th day along the cross section indicated by the solid line in Fig. 5.2b. Units are microbars per second, and positive areas (downward motion) are shaded.

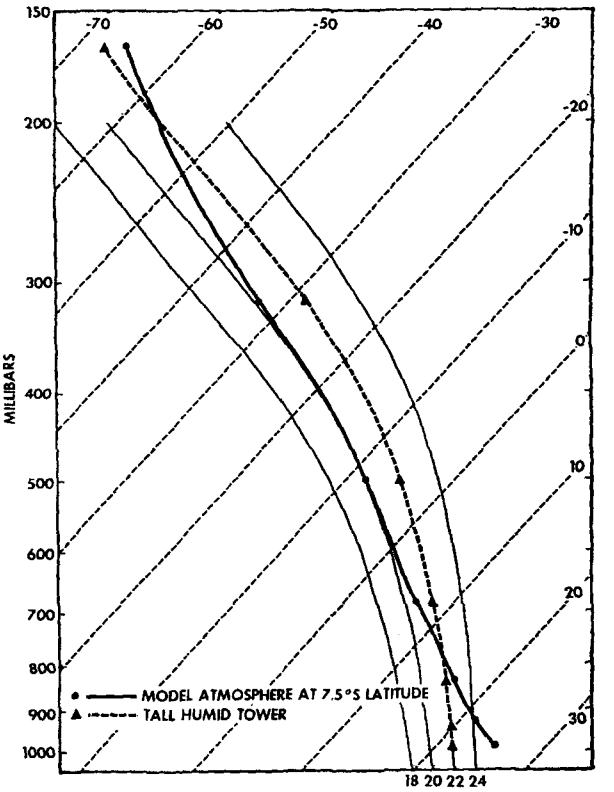

FIG. 5.8. Adiabatic diagram showing the vertical distribution of zonal mean temperature in the model tropics as a thick solid line. Temperature in the humid tower at the cyclone center is shown by a heavy dashed line. See caption of Fig. 3.3 for further explanation of this diagram.

decreases with time. Similar downward extension of the warm anomaly is often observed during the period of the development of hurricanes (Yanai, 1961). After the 247th day, the warm core starts decaying. The development and the subsequent decay of the warm core

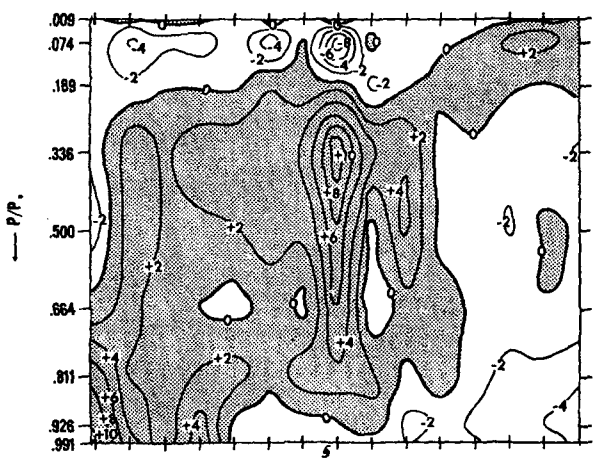

FIG. 5.9. The distribution of temperature deviation (°C) from the zonal mean on the 246th day along the cross section indicated by the solid line in Fig. 5.2b. Positive areas are shaded.

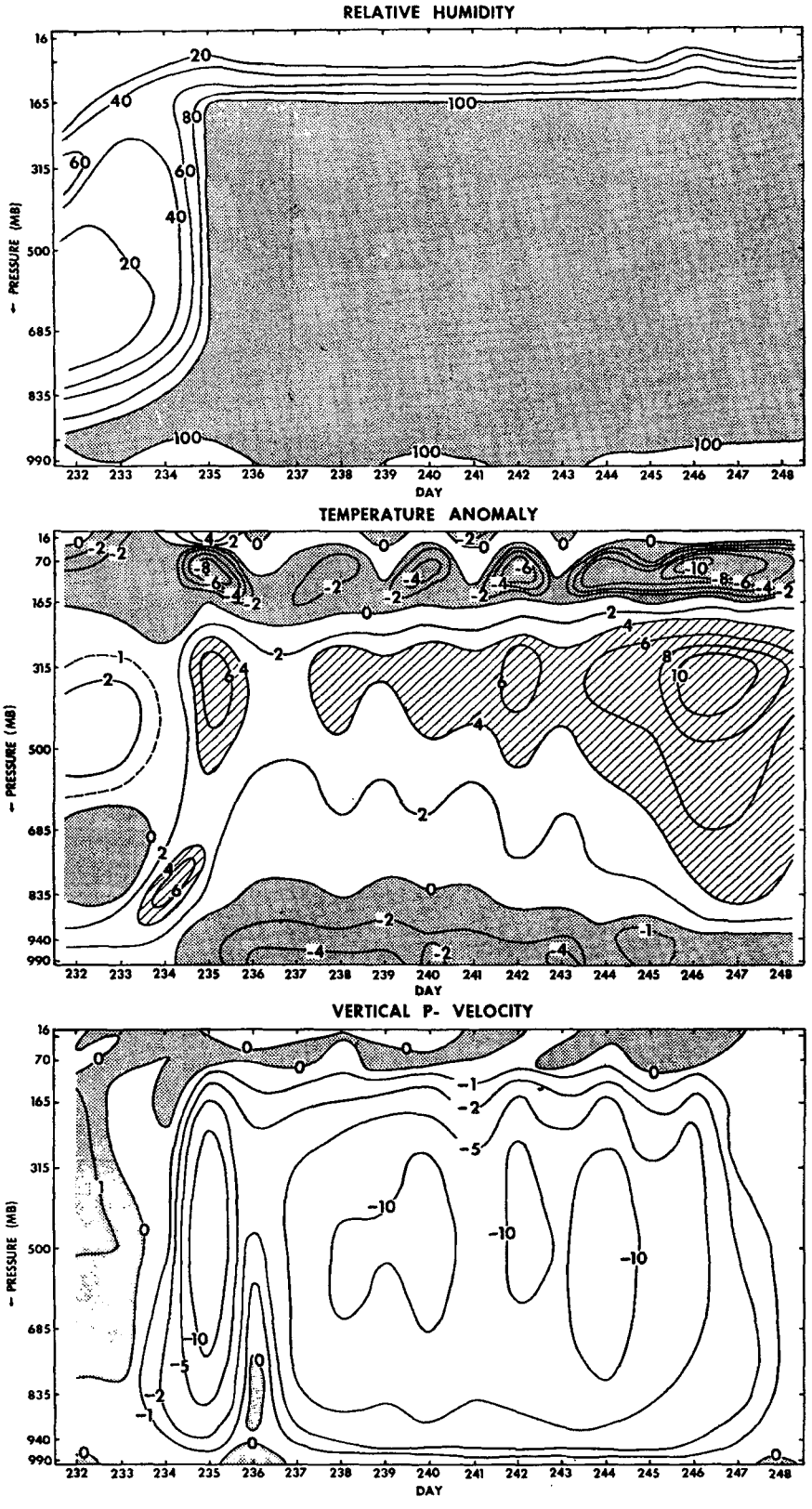

FIG. 5.10. Time sections of relative humidity (percent), temperature deviation from the zonal mean (°C), and vertical p velocity (μb sec^{-1}) at the grid point closest to the center of the tropical cyclone. The waviness of the contours with respect to time is caused by discrete shifts of the datum point from one grid point to another.

described above is accompanied by the intensification and then the weakening of the upward motion in the humid tower, and accordingly, by the increase and then the decrease in the rate of the release of potential energy. Therefore, the central pressure of the cyclone deepens when the warm core develops and fills when the warm core decays (see Fig. 5.4).

The evolution of the thermal structure of the core described above seems to be related to the rate of energy exchange between the ocean and the atmosphere. According to Fig. 5.10a, turbulent fluxes of energy (sensible heat and latent heat) from the ocean surface to the atmosphere at the grid point closest to the cyclone center predominate during the 239–245th day period when the development of the warm core is most pronounced. The magnitude of energy exchange becomes small on the 247th day when the warm core stops developing. In order to examine the mechanism of this energy exchange, the air-sea temperature difference at the grid point closest to the center of the cyclone is plotted with respect to time in the upper part of Fig. 5.10a. This figure indicates that the energy exchange has a large value when the air-sea temperature difference is significantly large but becomes small on the 247th day when the air-sea temperature difference is reduced to almost zero. Obviously, it is desirable to investigate the energy exchange in the whole area occupied by the cyclone rather than the energy exchange near the center of the cyclone. Nevertheless, these results suggest that the cold core over the sea surface created by the convective adjustment enhances the energy exchange between the ocean and the atmosphere and increases the temperature of the humid towers. Such an increase in the temperature of the humid tower causes the development of the tropical cyclone by increasing the release of available potential energy in the warm core of the upper troposphere.

According to Riehl and Malkus (1958), cumulonimbus clouds or shower clouds are not only effective in transferring heat upward but are also a mechanism for enhancing the transfer of heat from the sea to the atmosphere (see also Zipser, 1969). As is known, heavy convective precipitation often generates a downdraft. Their study indicates that the air in the downdraft arrives at the sea surface with a temperature appreciably lower than that of the sea. They therefore concluded that the air should be consequently warmed by the sensible heat flux from the warm underlying surface. The aggregate of such downdrafts could constitute a cold region similar to the cold core which resulted from the convective adjustment of the model. If so, the mechanism of the energy exchange suggested by Riehl and Malkus (1958) corresponds to the mechanism of the exchange taking place in the cyclones of the model tropics.

The analysis of the structure of the tropical cyclone described here suggests that the release of eddy available potential energy in the warm core created by the moist

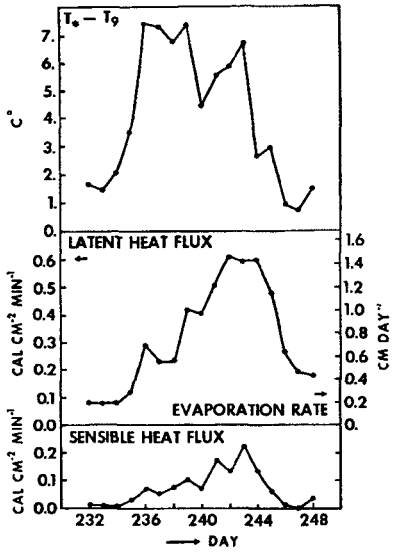

FIG. 5.10a. The rates of supply of latent and sensible heat from the ocean surface to the atmosphere at the grid point closest to the center of the tropical cyclone. The upper part shows the temperature difference between the sea surface and the lowest prognostic level (9) defined by Table 1.

convective adjustment is responsible for the development of the tropical cyclone. A similar conclusion was obtained by Manabe and Smagorinsky (1967). However, the tropical cyclone they obtained rarely developed a low pressure center such as the one described above. In their study, it was assumed that the earth's surface is wet but has no heat capacity. Accordingly, most of the air-earth temperature difference produced by the convective adjustment disappears instantaneously in order to satisfy the condition of the heat balance at the earth's surface. In the present study the sea surface temperature is assumed to be fixed. A comparison between the results from the two studies seems to indicate that a continuous supply of energy from the warm sea surface is necessary for development of tropical cyclones with central depressions of significant magnitude.

The analysis described so far shows how the condensation process controls the structure and the development of the tropical disturbances. Another way of identifying the effect of condensation processes is to compare the tropical disturbances of the moist model with those of the dry model. For this purpose, streamline maps of the dry model are shown in Fig. 5.11, which can be compared with those of the moist model shown in Fig. 5.1. In the lower troposphere of the dry model, wind vectors are very short and there are hardly any disturbances of significant intensity; whereas in the lower troposphere of the moist model, an intense shear line and tropical cyclones develop as previously described. In the upper troposphere, there are large-scale flow patterns in both model atmospheres. However, the flow field of the dry model is much less divergent (or more convergent) than that of the moist model, and the intensities of the disturbances of the dry model are

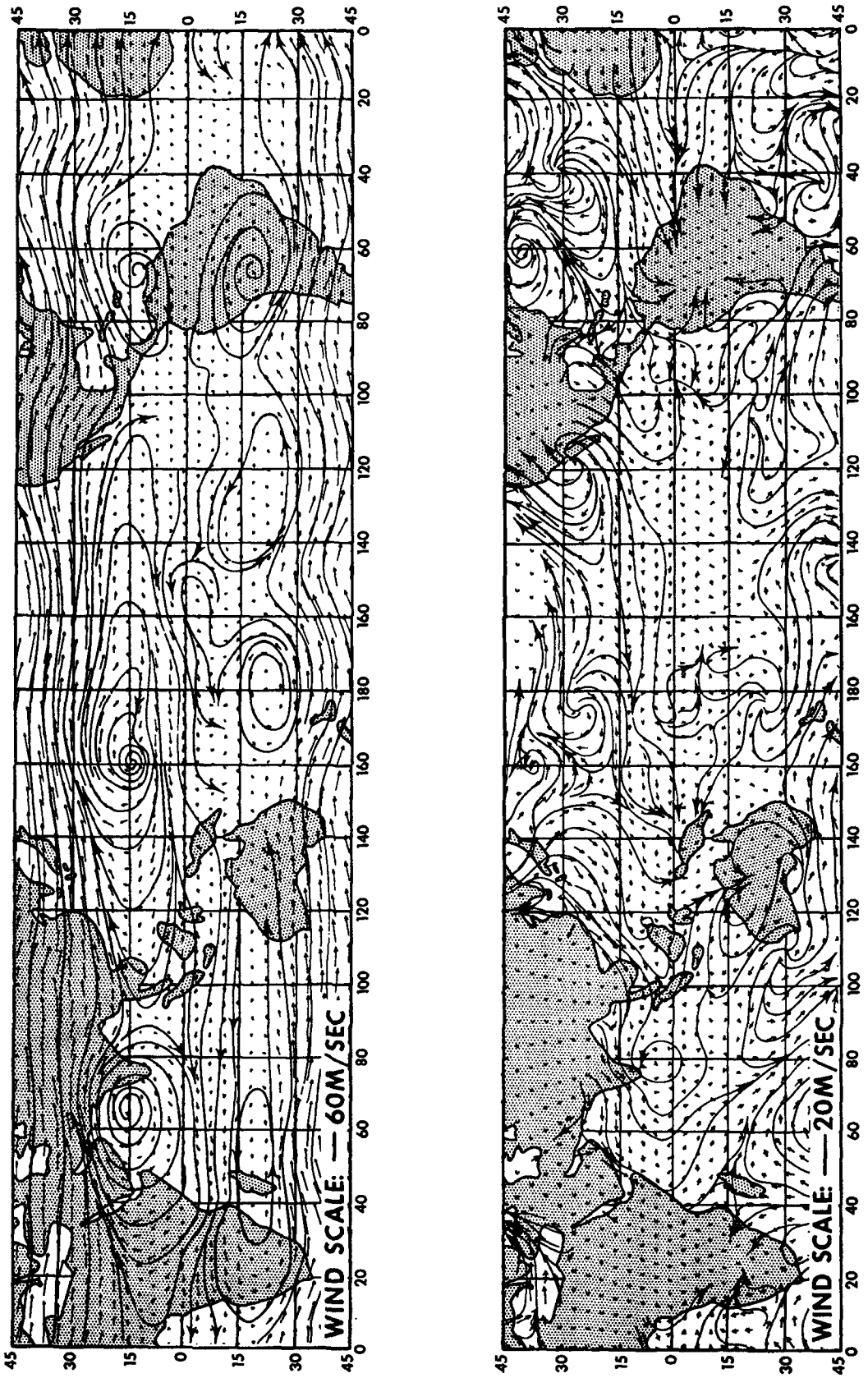

FIG. 5.11. Maps of streamlines and wind vectors on the 74th day of the integration of the dry model: upper half, 165-mb level; lower half, 990-mb level.

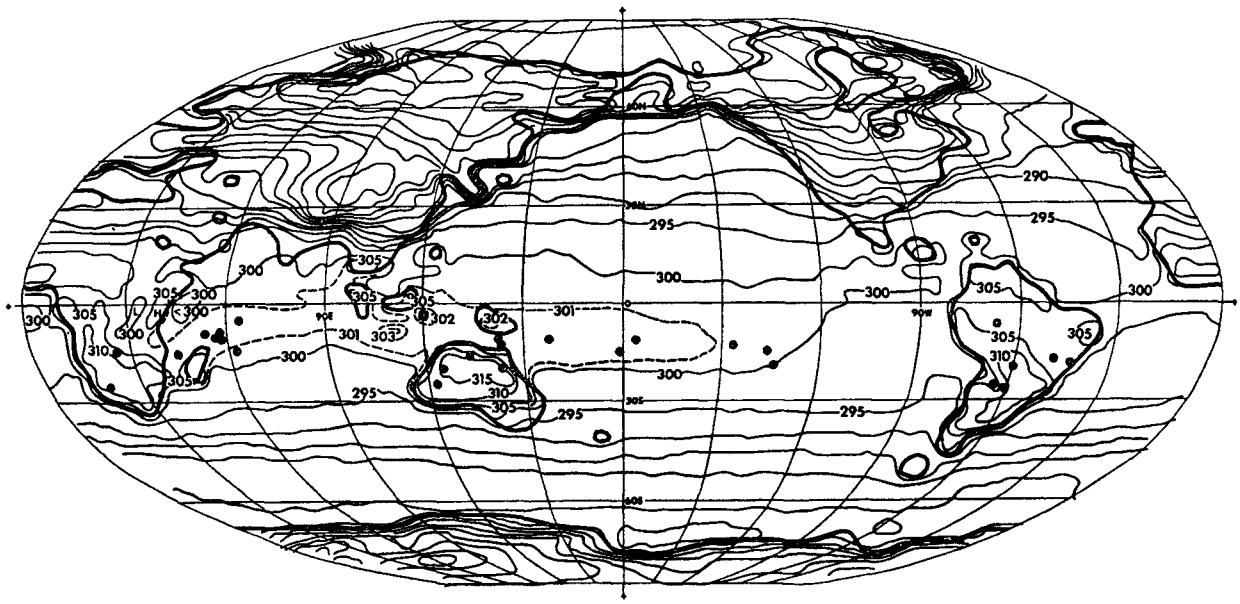

FIG. 5.12. Formation areas (black dots) of tropical cyclones with significant central pressure depression (≥ 2 mb) during the 120-day period starting from the 160th day of the integration of the moist model. Isotherms indicate temperature of earth's surface: over sea, February mean values (Hydrographic Office, 1944); over land, mean for 40-day period from the 302nd to the 341st day of the integration.

much less than those of the moist model. The differences between the features of the flow fields of the two models are consistent with the differences between the kinetic energy spectra of the two models discussed in Section 4.

In order to determine the areas favorable for the formation of cyclones in the model tropics, a statistical study of their formation has been carried out. Fig. 5.12 shows the locations of formation during a 120-day period of analysis. A tropical cyclone with a central depression ≥ 2 mb is considered for this analysis. The total number of formations is 40; 10 in the Indian Ocean, 13 in the Pacific, 7 over South America, and 10 in Australia. One can compare Fig. 5.12 with an illustration in Gray's (1968) paper which shows the frequency of formation of tropical storms in the actual tropics. It is interesting that the areas of frequent formation of cyclones in the oceanic regions of the model tropics coincide very well with the areas of frequent formation of tropical storms in the actual tropics during the Southern Hemisphere summer. It must be pointed out, however, that the cyclones in the model tropics cannot develop into intense tropical storms. In order to determine whether some of these cyclones could develop into tropical storms such as typhoons or hurricanes, it would be necessary to use a very fine grid of finite differencing near the center of these cyclones.

Fig. 5.12 indicates that tropical cyclones of the model also form in the desert areas of Australia. Although this result seems to be very unrealistic, a recent study by Simpson *et al.* (1968) indicates that tropical storms often initiate from the Sahara Desert during the summer season of the Northern Hemisphere. The formation of cyclones in deserts, therefore, may not be as unreasonable as it at first seemed.

The vortices, which are formed in the Australian desert, are very dry and weak and are quite different from the moist vortices described so far. The evolution

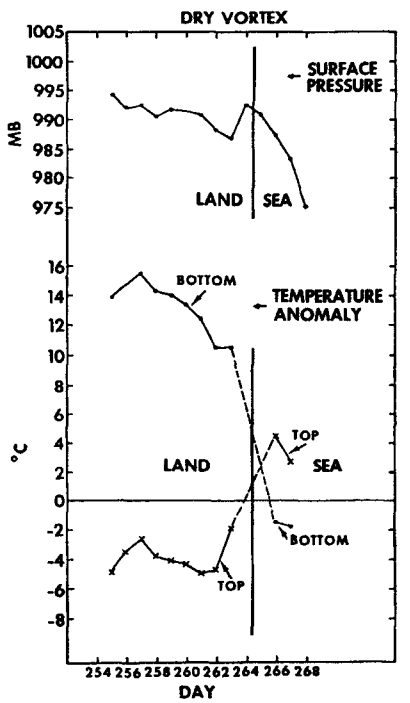

FIG. 5.13. Time variation of surface pressure at the grid point closest to the center of a cyclone formed in the Australian desert (upper), and time variation of the maximum temperature anomaly in the warm core and of the minimum temperature anomaly in the cold core (lower). (Here the word anomaly should be interpreted as the deviation from the zonal mean.) The dashed line portion of the graph indicates the transition period when the warm and cold cores are not clearly identifiable.

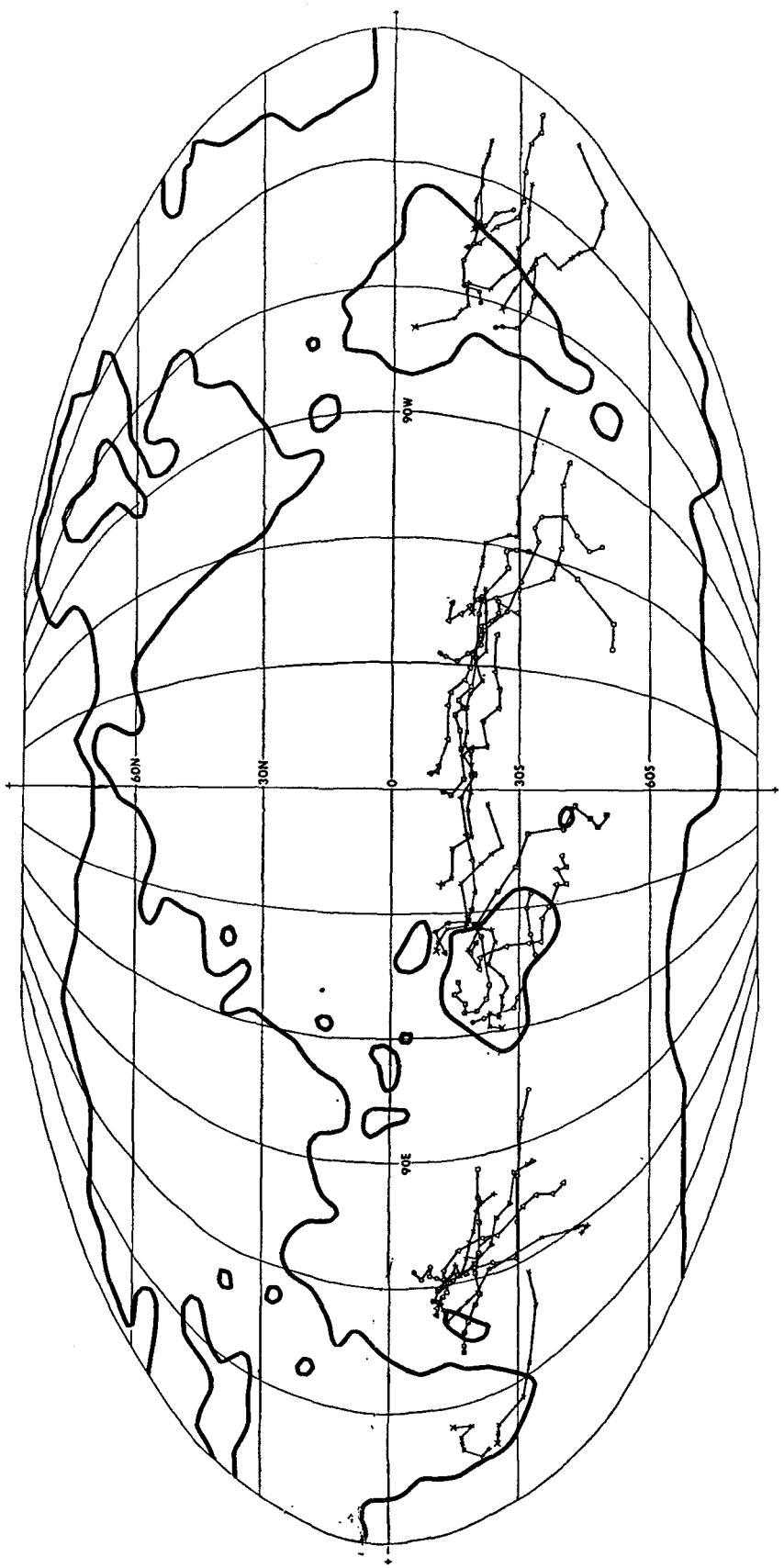

FIG. 5.14. Tracks of tropical cyclones from the points of origin indicated in Fig. 5.12. Symbols indicate positions at 1-day intervals.

of one example of such a vortex is shown in Fig. 5.13. On the desert the vortex is a shallow heat low contained below the 600-mb level. As soon as such warm air moves into the ocean, however, the upward motion driven by the solenoidal field creates a moist layer and accordingly triggers the moist convective adjustment. The rapid change in the thermal structure just after crossing of the land-sea boundary clearly indicates the execution of the moist convective adjustment. The weak, dry heat low quickly transforms into a weak, moist low with a warm core aloft and a cold core below. The rapid development of the central pressure follows as indicated in the upper part of Fig. 5.13.

The tracks of the cyclones, which are considered in the statistics of formation in Fig. 5.12, are shown in Fig. 5.14. The tracking of a cyclone was terminated when it moved into middle latitudes. According to this figure, the tropical cyclone moves poleward after its formation and fails to recurve. Westerlies, which appear in the upper troposphere of the model tropics (see Fig. 3.1), may be partly responsible for this lack of westward movement of tropical cyclones in the moist model atmosphere.

6. Energetics

Before discussing how the eddy kinetic energy of the disturbances described in the preceding sections is maintained, it is necessary to derive the energy equations.

The equation of the zonal mean of total kinetic energy k_T in the pressure coordinate system may be written as

$$\frac{\overline{\partial k_T}^{\lambda}}{\partial t} = -\overline{D(k_T)}^{\lambda} - \overline{\mathbf{V}\cdot\nabla_H\phi}^{\lambda} + \overline{\mathbf{V}\cdot\mathbf{F}}^{\lambda}, \tag{1}$$

where

$$k_T = \tfrac{1}{2}(u^2+v^2), \tag{2}$$

$$\overline{D(\ )}^{\lambda} = \frac{1}{a\cos\theta}\frac{\partial}{\partial\theta}[\cos\theta\cdot\overline{v(\ )}^{\lambda}] + \frac{\partial}{\partial p}[\overline{\omega(\ )}^{\lambda}], \tag{3}$$

t is time, a the radius of the earth, $\mathbf{V}$ the horizontal wind vector, u and v the east and northward components of the wind, respectively, ω vertical p-velocity, θ latitude, p pressure, ϕ geopotential height, and $\mathbf{F}$ a frictional force vector. The symbols $\overline{(\ )}^{\lambda}$ indicates the zonal mean of ( ). The equation of zonal kinetic energy k_Z is

$$\frac{\partial k_Z}{\partial t} = -\overline{D(k_Z)}^{\lambda} - \langle k_Z\cdot k_E\rangle - \overline{\mathbf{V}}^{\lambda}\cdot\nabla_H\overline{\phi}^{\lambda} + \overline{\mathbf{V}}^{\lambda}\cdot\overline{\mathbf{F}}^{\lambda}, \tag{4}$$

where

$$k_Z = \tfrac{1}{2}|\overline{\mathbf{V}}^{\lambda}|^2 = \tfrac{1}{2}[(\bar{u}^{\lambda})^2+(\bar{v}^{\lambda})^2]. \tag{5}$$

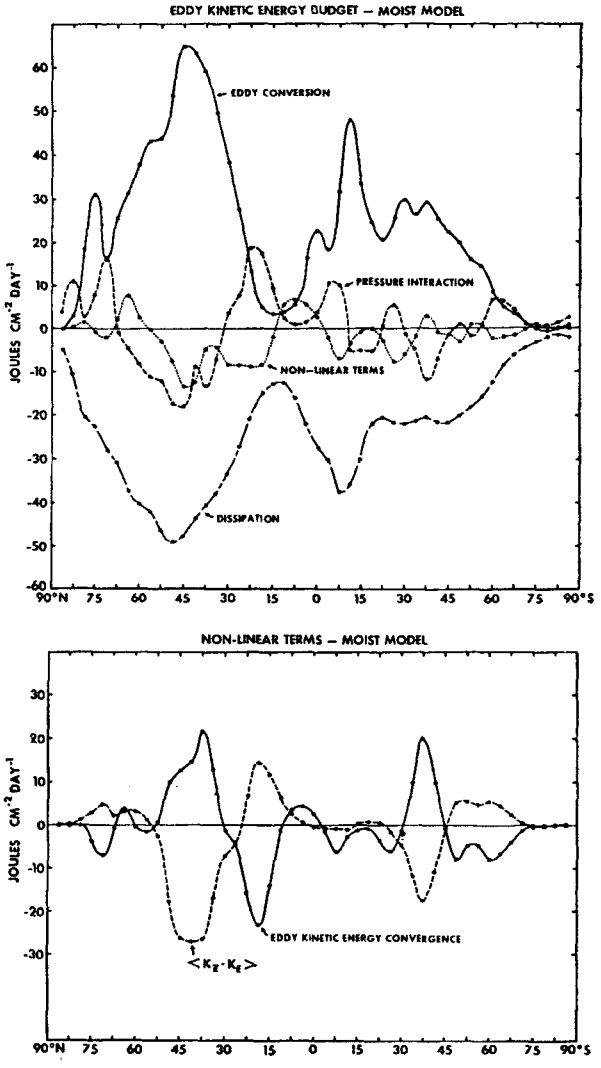

FIG. 6.1. Latitudinal distribution of vertical integrals of various components of the budget of eddy kinetic energy in the moist model atmosphere. As a result of truncation error involved in the computation of the energy budget, the sum of all contributions does not vanish. In the lower part of the figure, the nonlinear term is again shown, but here it is subdivided into two parts, i.e., $\langle k_Z\cdot k_E\rangle$ and the convergence of the transport of kinetic energy.

By use of the divergence operator defined by (3), the transformation term in (4) becomes[4]

$$\langle k_Z\cdot k_E\rangle = (\bar{u}^{\lambda}/\cos\theta)\overline{D(u'\cos\theta)}^{\lambda} + \bar{v}^{\lambda}[\overline{D(v')}^{\lambda} + (\tan\theta/a)\overline{(u')^2}^{\lambda}], \tag{6}$$

where ($'$) indicates the deviation from the zonal mean value. Inasmuch as $\bar{u}^{\lambda}\gg\bar{v}^{\lambda}$, the second term on the right-hand side of Eq. (6) is disregarded in the present study. Subtracting (4) from (1), one obtains the follow-

[4] Sometimes, $\langle k_Z\cdot k_E\rangle$ and k_E may be defined differently. See, for example, Section 6d of the paper by Mak (1969). His $\langle k_Z\cdot k_E\rangle$ and k_E are not the same as ours.

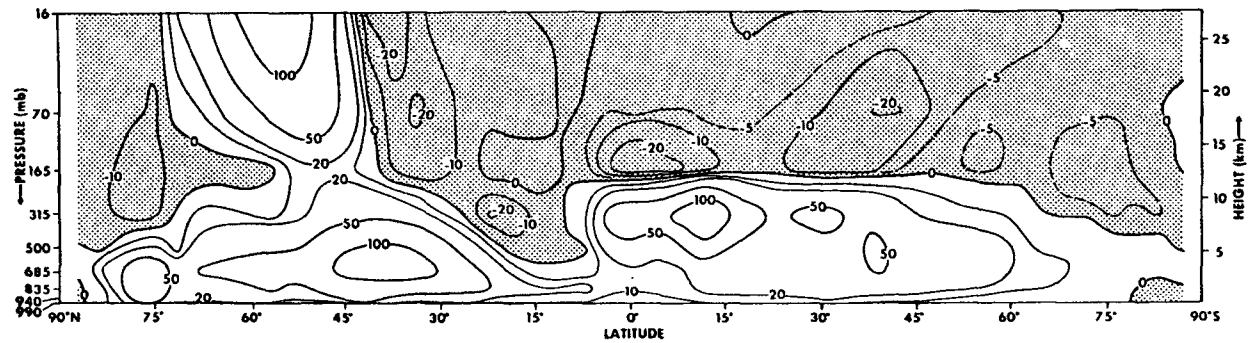

FIG. 6.2. The latitude-height distribution of eddy conversion, $\overline{(-\omega'\alpha')}^{\lambda}$, in the moist model atmosphere. Units are 10^{-3} J cm^{-2} mb^{-1} day^{-1}.

ing equation for the eddy kinetic energy[4]:

$$\frac{\overline{\partial k_E}^{\lambda}}{\partial t} = [-\overline{D(k_E)}^{\lambda} + \langle k_Z \cdot k_E \rangle] - \overline{\mathbf{V}' \cdot \nabla_H \phi'}^{\lambda} + \overline{\mathbf{V}' \cdot \mathbf{F}'}^{\lambda}, \quad (7)$$

where

$$k_E = k_T - k_Z = \bar{u}^{\lambda} u' + \bar{v}^{\lambda} v' + \tfrac{1}{2}[(u')^2 + (v')^2]. \quad (8)$$

In the following discussion, the sum of the first two terms enclosed in the square brackets will be called the nonlinear term, the third term, $\overline{(-\mathbf{V}' \cdot \nabla_H \phi')}^{\lambda}$, will be called the production term of eddy kinetic energy, and the fourth term, $\overline{\mathbf{V}' \cdot \mathbf{F}'}^{\lambda}$, will be called the "dissipation term." The nonlinear term can be separated into two terms, that representing the convergence of eddy kinetic energy transport, $\overline{[-D(k_E)]}^{\lambda}$, and the energy transfer from zonal to eddy kinetic energy, $\langle k_Z \cdot k_E \rangle$. Furthermore, the production term of eddy kinetic energy, $\overline{(-\mathbf{V}' \cdot \nabla_H \phi')}^{\lambda}$, may be subdivided into two parts, i.e.,

$$\overline{-\mathbf{V}' \cdot \nabla_H \phi'}^{\lambda} = -\overline{\omega'\alpha'}^{\lambda} - \overline{D(\phi')}^{\lambda}, \quad (9)$$

where the first term represents the conversion of eddy available potential energy and is called the "eddy conversion term." The second term represents the energy exchange by the pressure interaction and will be called the "eddy pressure interaction term."

The latitudinal distribution of the vertical integrals of the various components of the budget of eddy kinetic energy identified above are shown in Fig. 6.1. According to this figure, the most important source of eddy kinetic energy in the tropics (15N–15S) of the moist model is the conversion of eddy available potential energy. In order to examine the distribution of this term further, the latitude-height distribution of eddy conversion, $\overline{(-\omega'\alpha')}^{\lambda}$, is shown in Fig. 6.2. This figure indicates that the eddy conversion has a local maximum at about the 320-mb level of the model tropics. As we pointed out in the preceeding section, the upward motion increases the relative humidity, activates the moist convective adjustment, and creates a warm core structure in the upper and middle troposphere. Therefore, the upward motion converts the eddy potential energy there. The energy thus converted is transferred both upward and downward by the vertical component of the eddy pressure interaction. Such a vertical energy transport is evident in Fig. 6.3 which shows the latitude-height distribution of $\overline{(-\omega'\phi')}^{\lambda}$. The downward flux supplies energy to the planetary boundary layer where the rate of dissipation is large. On the other hand, the upward flux converges just below the equatorial tropopause and is responsible for the eddy kinetic

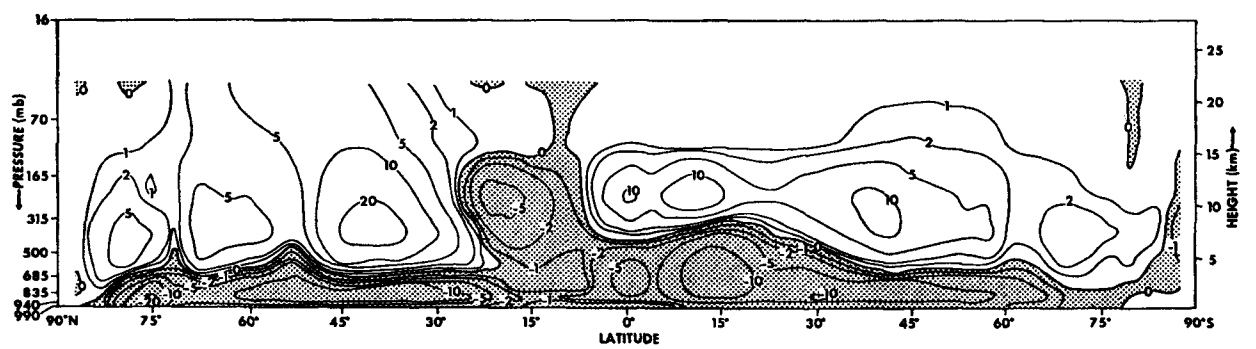

FIG. 6.3. The latitude-height distribution of the upward eddy flux of geopotential, $\overline{(-\omega'\phi')}^{\lambda}$, in the moist model atmosphere. Units are J cm^{-2} day^{-1}.

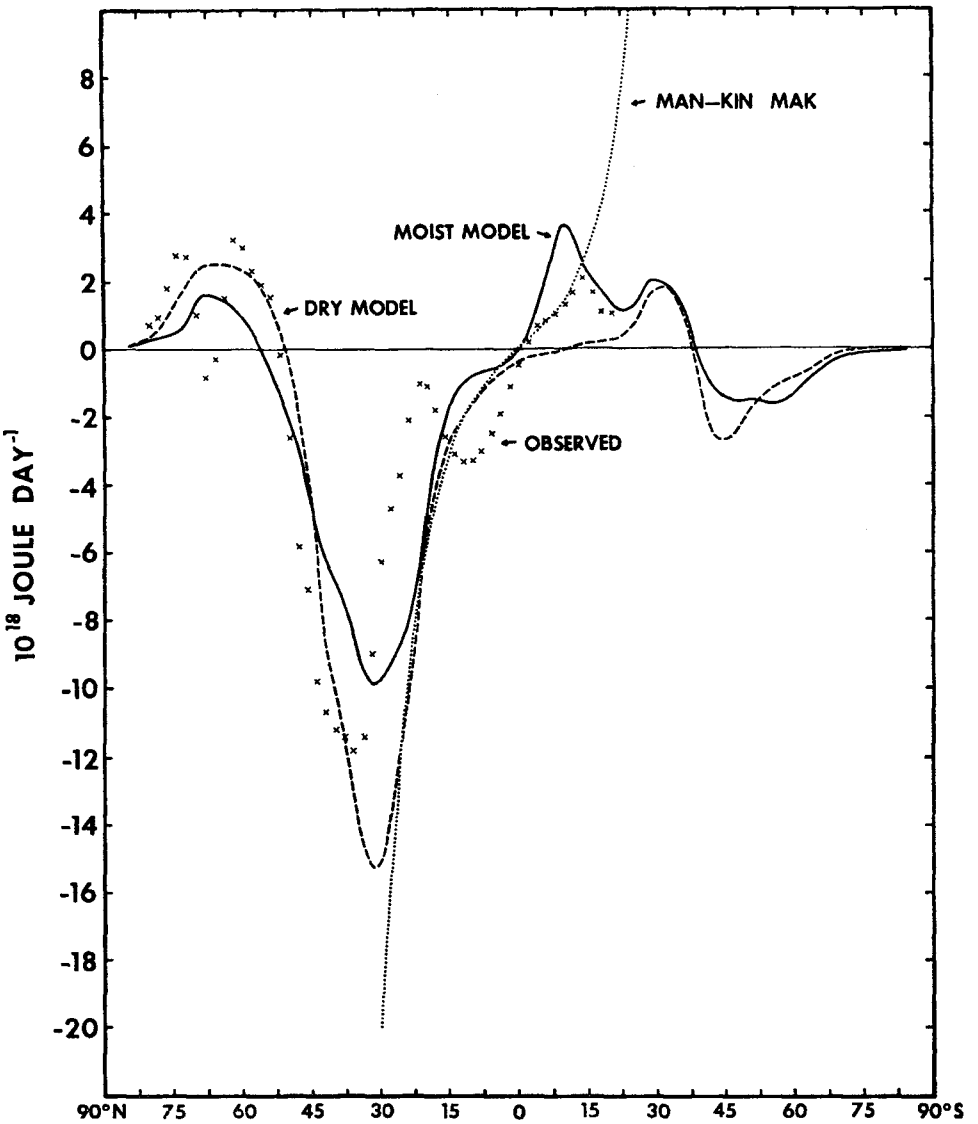

FIG. 6.4. The latitudinal distributions of the northward transports of energy by the eddy pressure interaction across a latitude circle in the model atmospheres. The distribution in the actual atmosphere estimated by Oort and Rasmusson (1970b) is shown by crosses; that obtained by Mak (1969) by dotted lines.

energy maximum at this level. It is interesting that a region of negative eddy conversion appears in the Northern Hemisphere subtropics of the model. As we shall demonstrate in the following paragraph, the energy supply by pressure interaction is important in the model subtropics.

Fig. 6.1 indicates that the horizontal eddy pressure interaction has a positive contribution to the production of eddy kinetic energy in the moist model tropics. The magnitude of its net contribution, however, is much smaller than that of the eddy conversion mentioned above. According to Fig. 6.4, which shows the latitudinal distribution of the northward energy transfer by the pressure interaction,

$$[(2\pi a \cos\theta)/g]\int_0^{p_{\text{surf}}} \overline{v'\phi'}^{\lambda}\, dp,$$

in various atmospheres, the eddy pressure interaction in the moist model Northern Hemisphere removes energy from middle latitudes and supplies energy mainly to high latitudes and the subtropics. The energy transfer into the tropics is relatively small; therefore, most of the convergence of the energy flux takes place around 20N and constitutes the major source of eddy kinetic energy there. The latitude-height distribution of the

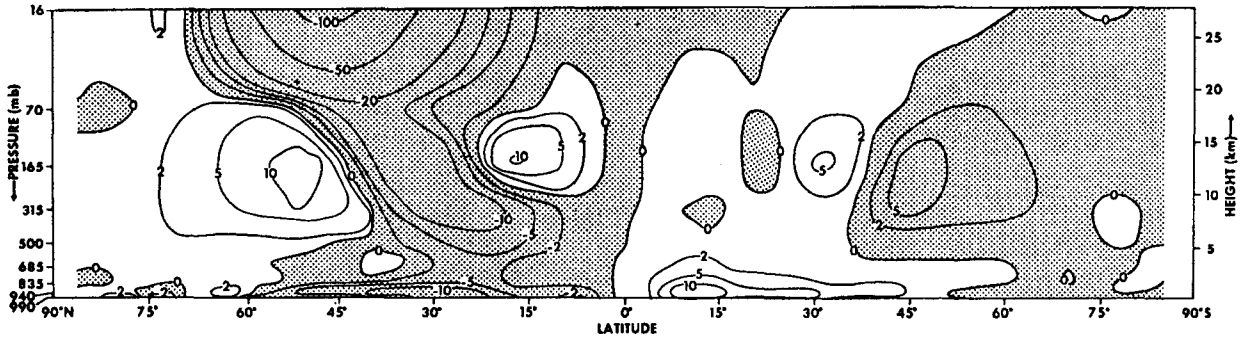

FIG. 6.4a. The latitude-height distribution of the zonal mean of the horizontal component of the eddy pressure interaction across a latitude circle, $\{[(2\pi a \cos\theta)g]\overline{v'\phi'}^{\lambda}\}$, for the moist model. Units are 10^{15} J mb^{-1} day^{-1}.

horizontal component of the eddy pressure interaction of the moist model shown in Fig. 6.4a also indicates the large subtropical convergence of energy flux in the upper troposphere in the Northern Hemisphere. As Fig. 6.1 indicates, the net contribution of the nonlinear term to the change of eddy kinetic energy in the moist model tropics is relatively small. The contribution of the nonlinear effect can be divided into two parts as indicated by Eq. (7). The latitudinal distributions of the two parts are shown in the lower half of Fig. 6.1.

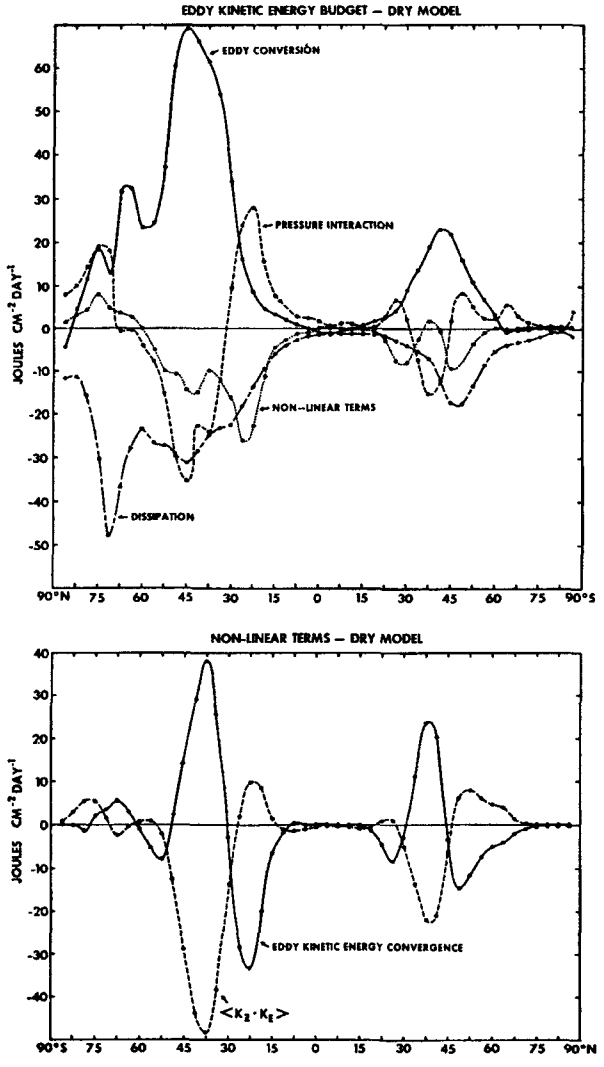

FIG. 6.5. Latitudinal distribution of the vertical integrals of the various components of the budget of eddy kinetic energy in the dry model atmosphere. For further explanation see the caption of Fig. 6.1.

In summary, the conversion of eddy available potential energy generated by the heat of condensation is the most important source of eddy kinetic energy in the moist model tropics and counterbalances the effect of dissipation. An essentially similar conclusion was obtained by Manabe and Smagorinsky (1967) in their study of the tropical circulation of a hemispheric model. Recently, Mak (1969) discussed the energetics of the tropics by using a simple two-layer model without considering the effect of condensation. He concluded that the pressure interaction is the most important factor in maintaining the eddy kinetic energy of the tropics. His conclusion seems to contradict the results presented here. Therefore, it was decided to analyze the budget of kinetic energy of the dry global model in order to comprehend Mak's results.

Fig. 6.5 shows the latitudinal distribution of the eddy kinetic energy budget in the dry model tropics. In the dry tropics the magnitudes of all terms are small, and the eddy kinetic energy is maintained by a very delicate balance among various terms with small contributions. The nonlinear term is subdivided into two parts which are shown in Fig. 6.5, both of which are very small in the dry tropics. Further examination of the figure indicates, however, that the pressure interaction has a small positive contribution in the dry tropics and is compensated mainly by dissipation. This result is in qualitative agreement with the result of Mak (1969). The magnitude of eddy conversion is much less than that in the moist tropics and is very small, again in agreement with Mak's result. This difference in the magnitude of the eddy conversion in the two model atmospheres accounts for the magnitude of the eddy kinetic energy in the dry tropics being much lower than that in the moist as shown in Section 4. In short, the

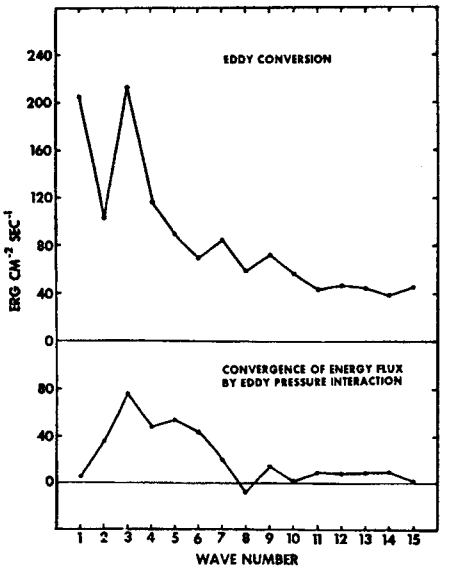

FIG. 6.6. Vertical integral of the spectral distribution of eddy conversion, $(\overline{-\omega'\alpha'})^p$, and that of the convergence of the energy flux by eddy pressure interaction in the moist model tropics (15N–15S).

difference between Mak's conclusions and ours stems from the difference between the dry and the moist models. Therefore, the validity of our conclusion depends upon our ability to simulate the effects of the moist processes.

As Fig. 6.4 indicates, the pressure interaction transfers energy from middle latitudes to the subtropics of the dry model and constitutes a major source of energy there. Again, this result is in qualitative agreement with Mak's results although the magnitude of the pressure interaction which Mak obtained is larger than that of the dry model. As previously indicated, a similar feature is evident in the Northern Hemisphere of the moist model atmosphere. Therefore, it is highly probable that the energy transfer from middle latitudes by pressure interaction contributes significantly to the maintainance of the eddy kinetic energy in the actual subtropics (15–30° latitude).

The spectra of eddy kinetic energy in the moist model tropics shown in Fig. 4.2 points out the predominance of long waves of planetary scale particularly in the upper troposphere. In order to find out how the eddy kinetic energy of such long waves is maintained, the vertical integral of the spectral distribution of the conversion of eddy available potential energy[5] and the vertical integral of the spectral distribution of the pressure interaction[5] in the moist model tropics are shown in Fig. 6.6. Since the spectrum of eddy conversion has a very long tail towards high wavenumbers, Fig. 6.6a is constructed to show the entire spectrum.

[5] In section 6B of their paper, Manabe *et al.* (1970) describe how one can compute the spectral distributions of conversion and of pressure interaction.

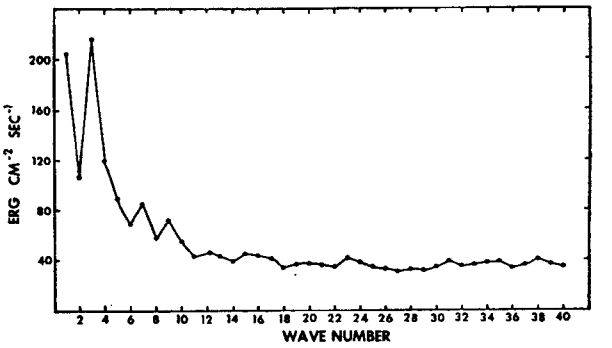

FIG. 6.6a. Vertical integral of the spectral distribution of eddy conversion in the moist model tropics (15N–15S). Same as shown in Fig. 6.6, but extended to higher wavenumbers.

The existence of such a long tail implies the prevalence of eddy conversion at high wavenumbers. It is clear, however, that the eddy conversion is most prominent at very low wavenumbers, particularly at wavenumber 3.

The pressure interaction also contributes to the production of eddy kinetic energy at very low wavenumbers. The contribution of pressure interaction, however, is much smaller than that of eddy conversion in the moist model tropics. The spectral distribution of energy transport by pressure interaction in the moist atmosphere is shown in Fig. 6.7. In the Northern

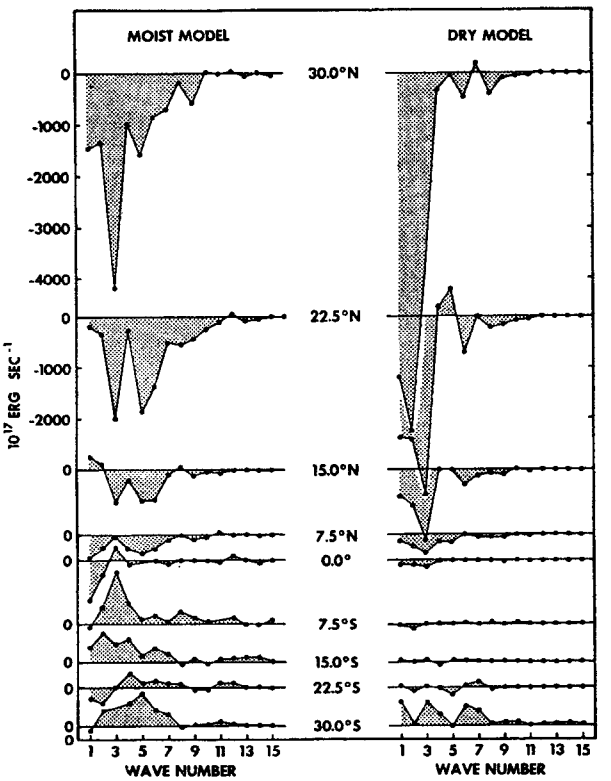

FIG. 6.7. Spectral distributions of the northward transport of energy across various latitude circles by pressure interaction in the moist and dry atmospheres.

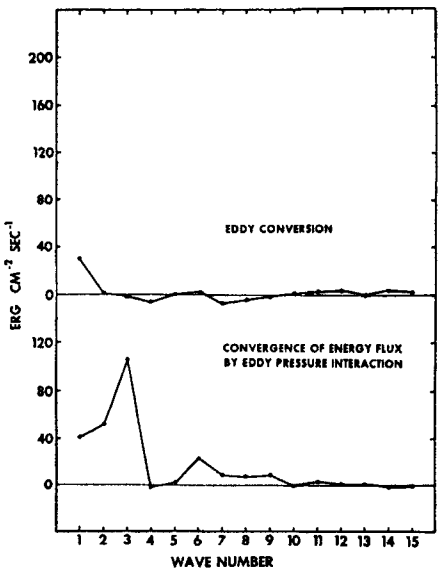

FIG. 6.8. Vertical integral of the spectral distribution of the two components of eddy kinetic energy budget in the dry model tropics (15N–15S). For further details see Fig. 6.6.

Hemisphere, the equatorward flux of pressure interaction at very low wavenumbers occurs in both the subtropics and the tropics and results in the production of the eddy kinetic energy mentioned above.

The energetics of the dry model are also analyzed in wavenumber space so that they can be compared with the energetics of the moist model. The vertical integrals of the spectra of eddy conversion and pressure interaction in the tropics of the dry model are shown in Fig. 6.8. As mentioned, pressure interaction is mainly responsible for maintaining the eddy kinetic energy in the tropics of the dry model. It acts as a source of eddy kinetic energy at very low wavenumbers but not at high wavenumbers. The spectral distribution of the horizontal energy flux by the pressure interaction in the dry model atmosphere is shown in the right-hand side of Fig. 6.7. This figure indicates a large equatorward flux at wavenumbers 1, 2 and 3, particularly in the Northern Hemisphere. Although the major part of the flux convergence takes place in the subtropics, some convergence takes place in the tropics and aids in maintaining the planetary-scale disturbances in the upper troposphere of the dry tropics. In summary, the energy flux from higher latitudes is chiefly responsible for maintaining the kinetic energy of the very long waves in the tropics and the subtropics of the dry model. The contribution of the eddy conversion is negligible. This may be the reason why the eddy kinetic energy in the dry model tropics has a much lower value than in the actual tropics, whereas the eddy kinetic energy in the moist model tropics has a realistic value (see the Appendix, sub-section b).

As pointed out in Section 3, the planetary-scale, time-mean flow pattern in the upper troposphere of the moist tropics has an interesting correspondence with that in the upper troposphere of the dry tropics, although the former has much more eddy kinetic energy than the latter. Furthermore, Fig. 4.2 indicates that the shape of the eddy kinetic energy spectrum in the upper troposphere of the moist tropics is very similar to that in the similar region of the dry tropics. For example, the eddy kinetic energy of the meridional wind reaches a maximum at wavenumber 3 and that of the zonal wind attains a maximum value at wavenumber 1 at the 165-mb level in both the dry and the moist tropics. These similarities seem to indicate that the flow patterns of planetary scale in the moist model tropics are strongly affected by the factors controlling the circulation in the dry tropics such as the interaction with higher latitudes. It must be emphasized, however, that the kinetic energy of the planetary-scale disturbances in the moist model tropics are chiefly maintained by the release of eddy available potential energy generated by the heat of condensation.

7. Angular momentum transport by large-scale eddies

a. Eddy transport

Recently, Kidson *et al.* (1969) found that large-scale eddies transport angular momentum from the winter hemisphere to the summer hemisphere in the upper troposphere of the tropics. The latitude-height distribution of the northward transport of angular momentum by both the transient and standing eddies during winter is computed from their results and is shown in Fig. 7.1.[6] This figure clearly illustrates the large cross-equatorial transport mentioned above. Similar cross-equatorial transport is evident in the upper half of Fig. 7.2, which shows the distribution of angular momentum transport by the large-scale eddies in the moist model atmosphere.[7]

The comparison between Figs. 7.1 and 7.2 indicates that the magnitude of the maximum transport in the moist model tropics is not very different from that in the actual tropics estimated by Kidson *et al.* (1969). Such a cross-equatorial flux is missing in the distribution of the eddy transport in the dry model atmosphere, which is shown in the lower half of Fig. 7.2. These results from the dry and the moist model experiments indicate

[6] The northward transport of momentum by both the transient and the standing eddies is defined by

$$2\pi(a\cos\theta)^2\left[\overline{(u-\bar{u}^t)\cdot(v-\bar{v}^t)}^{t\lambda}+\overline{(\bar{u}^t-\bar{\bar{u}}^{t\lambda})(\bar{v}^t-\bar{\bar{v}}^{t\lambda})}^{\lambda}\right]. \quad (10)$$

[7] The transport of angular momentum by large-scale eddies is given by

$$2\pi(a\cos\theta)^2\overline{(u-\bar{u}^{\lambda})\cdot(v-\bar{v}^{\lambda})}^{t}. \quad (11)$$

Note that the eddy transport defined here is slightly different from the transport defined by Eq. (10) for both the standing and transient eddies. The difference is equal to

$$2\pi(a\cos\theta)^2\overline{(\bar{u}^{\lambda}-\bar{\bar{u}}^{t\lambda})\cdot(\bar{v}^{\lambda}-\bar{\bar{v}}^{t\lambda})}^{t}, \quad (12)$$

i.e., the transport by the transient meridional circulation.

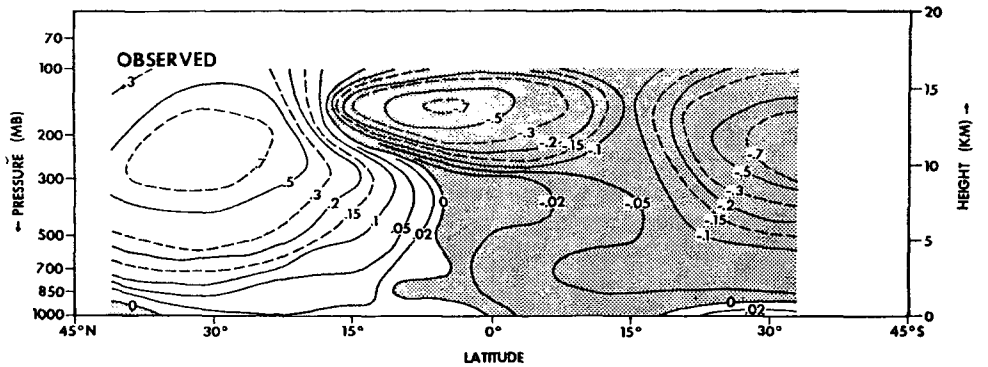

FIG. 7.1. Latitude-height distribution of the observed northward transport of angular momentum across a latitude circle by both transient and standing eddies (Kidson *et al.*, 1969). Units are 10^{29} gm cm^2 sec^{-1} day^{-1} mb^{-1}.

that the selective heating due to condensation is responsible for generating the large-scale disturbances which transport angular momentum across the equator of the moist model. The existence of the cross-equatorial transport in both the moist model and actual tropics may be an indication that the moist processes are incorporated properly into the moist model.

Further inspection of Fig. 7.2 indicates that, in middle latitudes of the moist model, the poleward eddy transport of angular momentum is unrealistically small. In the Appendix (sub-section c), it will be shown that the increase in the resolution of the horizontal finite differences eliminates this unrealistic feature to a certain degree.

b. Budget of absolute angular momentum

In order to examine the contribution of the cross-equatorial eddy transport mentioned above to the budget of angular momentum in the moist model tropics, Fig. 7.3 is constructed. In this figure, the rates of change of the absolute angular momentum due to meridional circulation and large-scale eddies in the moist model atmosphere are shown as a function of

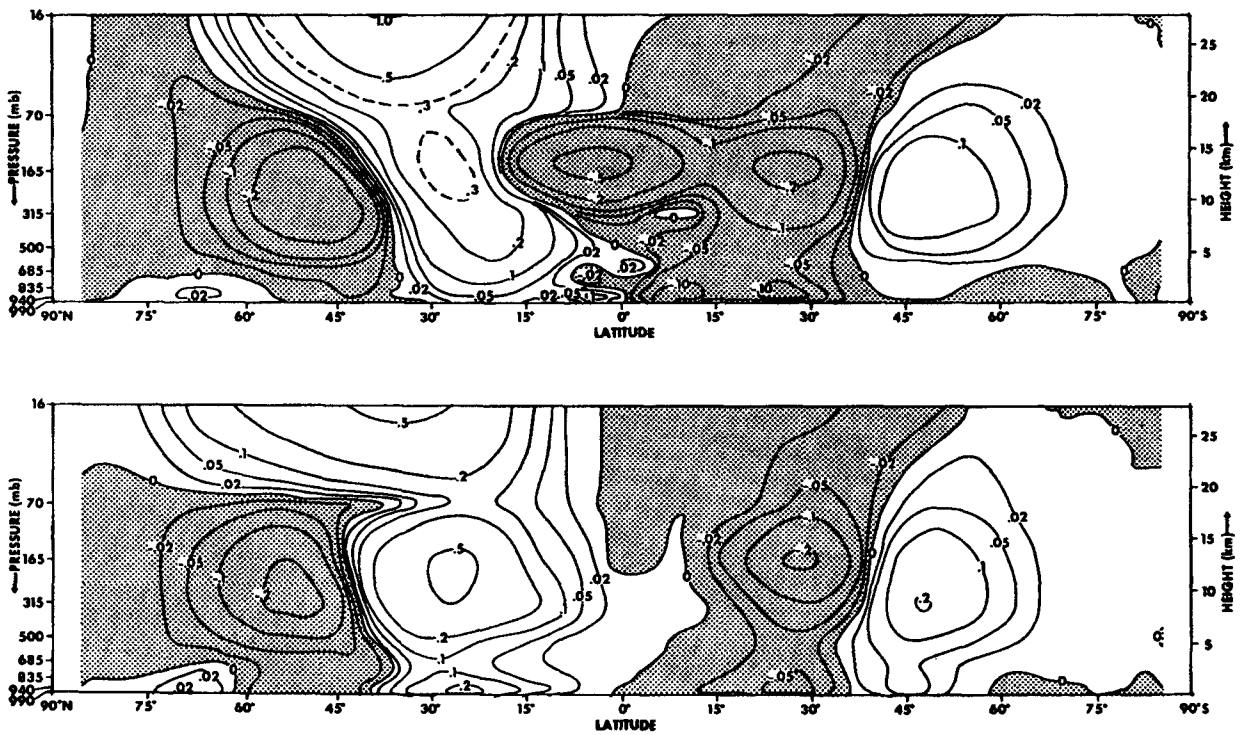

FIG. 7.2. Latitude-height distribution of the computed northward transport of angular momentum across a latitude circle by large-scale eddies in the model atmospheres. Units are 10^{29} gm cm^2 sec^{-1} day^{-1} mb^{-1}. Upper half, the moist model; lower half, the dry model.

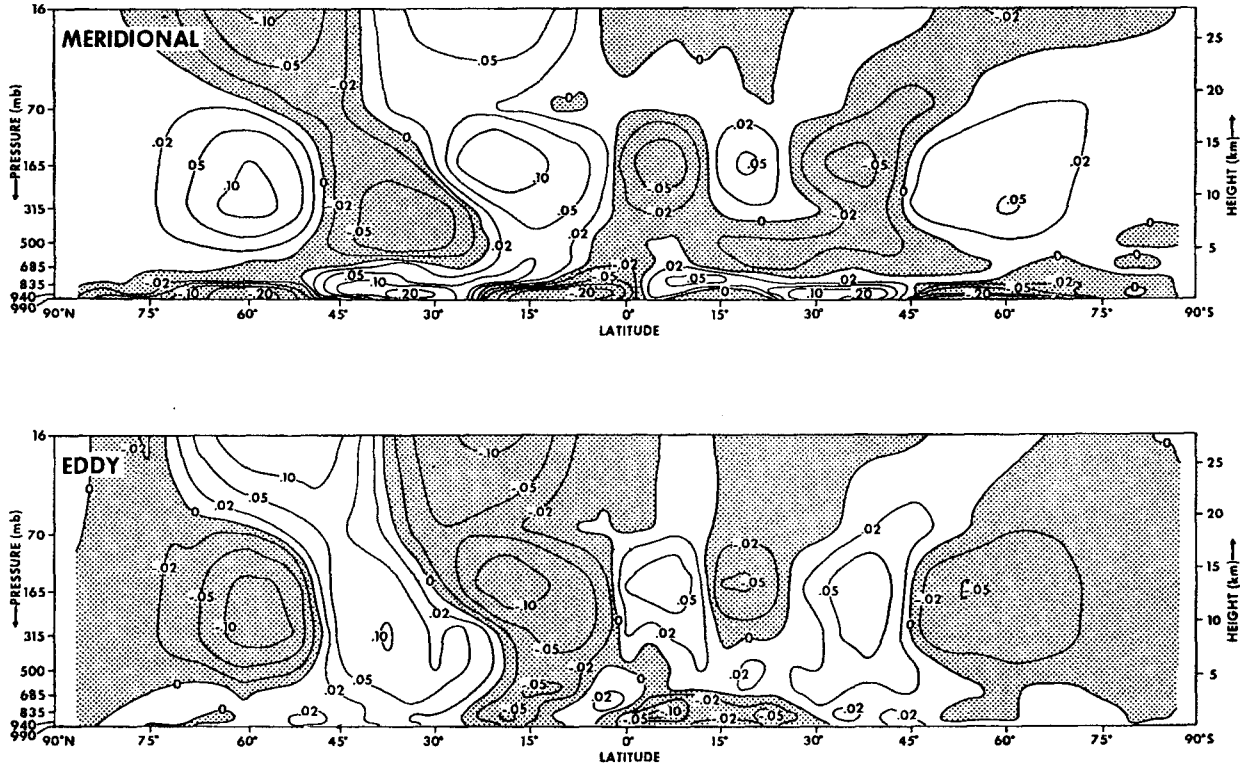

FIG. 7.3. The rate of change of absolute angular momentum in the moist model atmosphere due to various factors. Units are 10^{12} gm cm^2 sec^{-1} day^{-1} mb^{-1}. Upper half, meridional circulation; lower half, eddies.

latitude and height. This figure shows that, in the upper troposphere of the moist model tropics, the meridional circulation tends to reduce the absolute angular momentum just south of the equator and to increase it just north of the equator. These tendencies are almost compensated by the cross-equatorial eddy transport. In the lower troposphere, the contribution of the meridional circulation has an opposite sign from that in the upper troposphere and is almost compensated for by the effect of the sub-grid scale (vertical) mixing of momentum rather than by the effect of large-scale eddies.

According to Fig. 3.2, an intense Hadley cell transports mass across the equator from the summer to the winter hemisphere in the upper troposphere of the tropics. Using the concept of the conservation of absolute angular momentum, one can show that such a cross-equatorial flow can generate very strong easterlies at the equator. Recently, Dickinson[8] demonstrated, by use of his simple theoretical model, that the intensity of the easterlies in the upper troposphere becomes realistic if the effect of angular momentum transport by the large-scale eddies is taken into consideration. In other words, the cross-equatorial transport of angular momentum by large-scale eddies seems to play an important role in suppressing the intensity of the easterlies in the upper troposphere of the tropics during the period when the cross-equatorial current predominates.

8. Summary and conclusions

Various features of the general circulation of the tropics during January are successfully simulated by the numerical integration of the global general circulation model developed at the Geophysical Fluid Dynamics Laboratory of ESSA. For example, the general features of the flow field around the intertropical convergence zone of the model are highly realistic, and the intensities of the Hadley cells agree well with those estimated by Oort and Rasmusson (1970a).

In order to identify the effects of the condensation process in maintaining the general circulation of the tropics, the results from the moist model incorporating the effects of selective heating of condensation are compared with those from the dry model without these effects. As a result of this comparison, the factors which control the general circulation of the dry model seem to be mainly responsible for determining the location of the convergence zones in the moist tropics. The heat of condensation, however, increases the general intensity of the convergence by a factor of ~ 4.

The tropical cyclone, which has a warm core in the upper troposphere and a cold core in the lower troposphere, forms along the shear lines in the tropics of the

[8] Dickinson, R. E., 1969: Analytic models for zonal winds in the tropics including coupling with planetary waves. Paper presented at the Conference on the Global Circulation of the Atmosphere, London, 25–29 August.

moist model. The conversion of the available potential energy in the warm core region helps maintain the kinetic energy of the disturbances. As the cyclone develops, the warm core extends downward and the cold core shrinks as a result of the energy supply from the underlying ocean surface. Probably because of the coarse resolution of finite differences, the central depression of pressure seldom exceeds 20 mb. It is interesting, however, that the ocean areas of the moist model favorable for the formation and development of tropical cyclones agree with those of the actual ocean favorable for the formation of tropical storms. The energy supply from the warm sea surface to the cold core mentioned above seems to be necessary for such development.

The tropical cyclones described above have a characteristic scale of 2000–4000 km and are pronounced in the lower troposphere of the moist model. In the upper troposphere of the moist model tropics, the eddy kinetic energy is at a maximum and disturbances with planetary scale predominate. The analysis of the energetics shows that the conversion of the eddy available potential energy generated by the heat of condensation is chiefly responsible for the development of these disturbances. The energy supply from higher latitudes through the pressure interaction plays a secondary role. It is, however, an important source of eddy kinetic energy in the subtropics of the moist model.

In the dry model tropics, the conversion of the eddy potential energy has a small negative value. Accordingly, the eddy kinetic energy is very small in the lower troposphere, and tropical cyclones such as those described above do not form. In the upper troposphere, the disturbances with planetary scale do appear as a result of the pressure interaction with higher latitudes. The magnitude of eddy kinetic energy, however, is about three times smaller than in the moist model tropics and is much less realistic (see Appendix, sub-section b).

The long waves in the upper troposphere of the moist model tropics seem to be responsible for the transport of angular momentum from the winter to the summer hemisphere and strongly affect the budget of angular momentum in the upper troposphere of the moist model tropics. Similar cross-equatorial eddy transport is also found in the actual tropics. On the other hand, such a cross-equatorial eddy transport is not evident in the dry model tropics.

In conclusion, the structure and amplitude of the disturbances in the moist model tropics seem to be much more realistic than those in the dry model. Therefore, it is highly probable that the selective heating of condensation plays a major role in maintaining the disturbances with planetary scale as well as tropical cyclones with shorter wavelength in the actual tropics.

Acknowledgments. The authors gratefully acknowledge the many useful suggestions provided by Dr. Y. Kurihara for improving the model and enabling us to carry out a successful integration. We wish to express our appreciation to Drs. J. Smagorinsky and I. Orlanski for their excellent ideas for analysis and experimental design and to Dr. K. Miyakoda for his very constructive criticism during the entire project. We are indebted to Drs. A. Oort, E. Rasmusson and H. van Loon for permitting us to use their results before publication and to Mr. R. Wetherald for programming the computations of the hydrologic scheme in the model and for assistance in the analysis of the results. We also wish to thank the following programmers who contributed substantially to the codes for the model and the analysis computation: Mrs. W. Carlton, and Messrs. H. Stambler, R. Moyer, P. Baker, D. Johnson and D. Daniel.

APPENDIX

Some Results from the High-Resolution Model

According to the discussion in Section 5, a grid spacing of 417 km for the horizontal finite differences is too large to properly resolve the disturbances appearing in the model tropics. Using the results from the time integration of a hemispheric model, Manabe *et al.* (1970) showed that the increase in resolution significantly affects the energetics of very long as well as short waves. Therefore, a further increase in resolution is necessary to obtain satisfactory results. After completing the analysis of the low-resolution model, we repeated the experiment using a high-resolution model in order to get some idea as to the damage done by the coarseness of the finite difference grid. Here we shall describe briefly some of the results from this experiment. The grid spacing of the high-resolution model is half as large as that of the low resolution model. All other parameters are assumed to be identical for both models. Since the high-resolution moist model has 48 grid points between the pole and the equator, it is called the N48M model for simplicity of identification. Similarily, the low-resolution moist model is called the N24M model. Table A1 shows the grid lengths of both models at selected latitudes.

The state of the N24M atmosphere on the 302nd model day was chosen as an initial condition for the time integration of the N48M model. Fig. A1 shows the time variation of the global mean values of eddy kinetic

TABLE A1. The grid lengths (km) of the two models.

Location		Model N48M	Model N24M
Pole	Δ Longitude	327	655
	Δ Latitude	208	417
45N, S	Δ Longitude	295	590
	Δ Latitude	208	417
Equator	Δ Longitude	208	417
	Δ Latitude	208	417

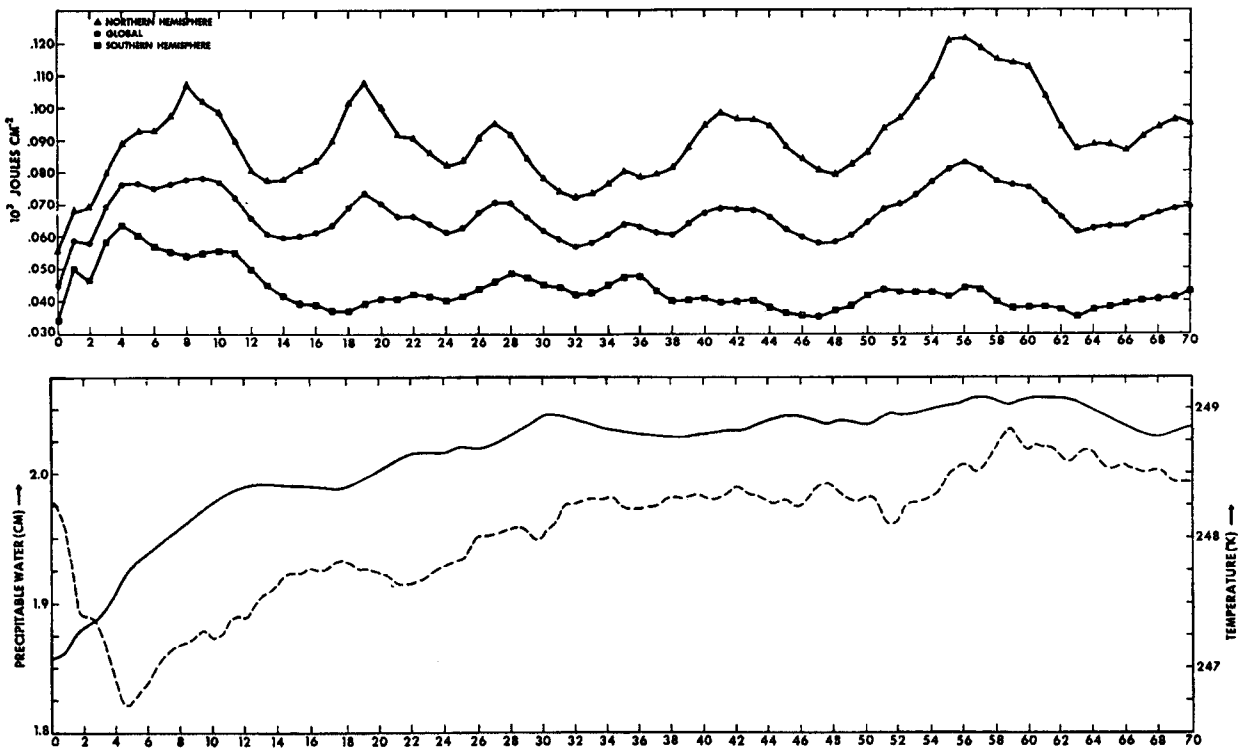

FIG. A1. Upper graph: time variation of eddy kinetic energy in the N48M atmosphere. Global mean and hemispheric means are shown. Lower graph: time variation of global means of temperature (solid line) and precipitable water (dashed line).

energy, temperature and precipitable water during the 70-day period of the integration. Obviously, it is desirable to extend the integration for a longer period of time in order to approach more closely a state of quasi-equilibrium. However, we terminated the integration on the 70th day because of the enormous amount of machine time required. Various quantities, which are shown here, represent the average state over the 36-day period starting from the 35th model day unless specified otherwise.

a. Zonal wind

Fig. A2 shows the latitude-height distribution of the zonal wind in the N48M atmosphere. According to this figure, the features of the easterlies in the troposphere of the model tropics are in agreement with those in the actual atmosphere shown in the upper half of Fig. 3.1. On the other hand, in the N24M atmosphere, weak westerlies appear in the upper troposphere of the tropics as was pointed out in Section 3. The cause of this difference between the two models is not obvious.

b. Eddy kinetic energy

In Fig. A3, the distribution of eddy kinetic energy in the N48M atmosphere is compared with that in the actual atmosphere which was obtained by Oort and Rasmusson (1970b) for the month of January. The definition of eddy kinetic energy, which is used for this

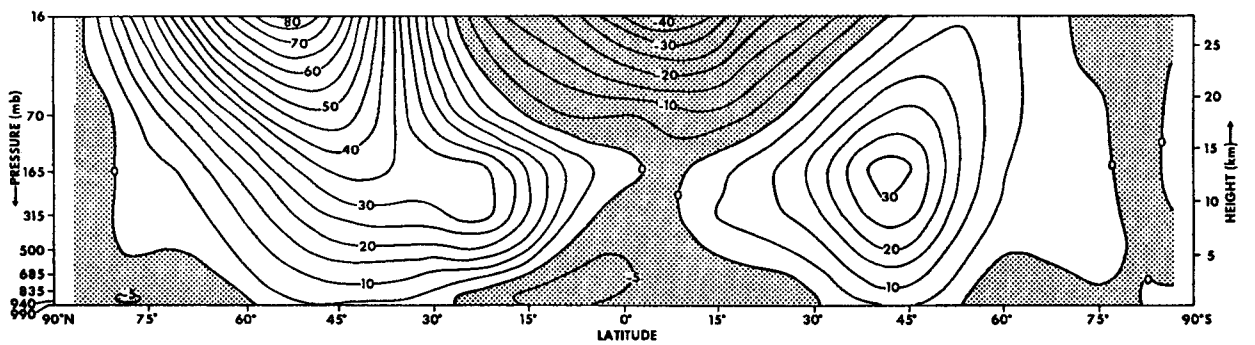

FIG. A2. Latitude-height distribution of the zonal mean of the zonal wind in the N48M atmosphere. Regions of easterly wind are shaded. Units are m sec^{-1}.

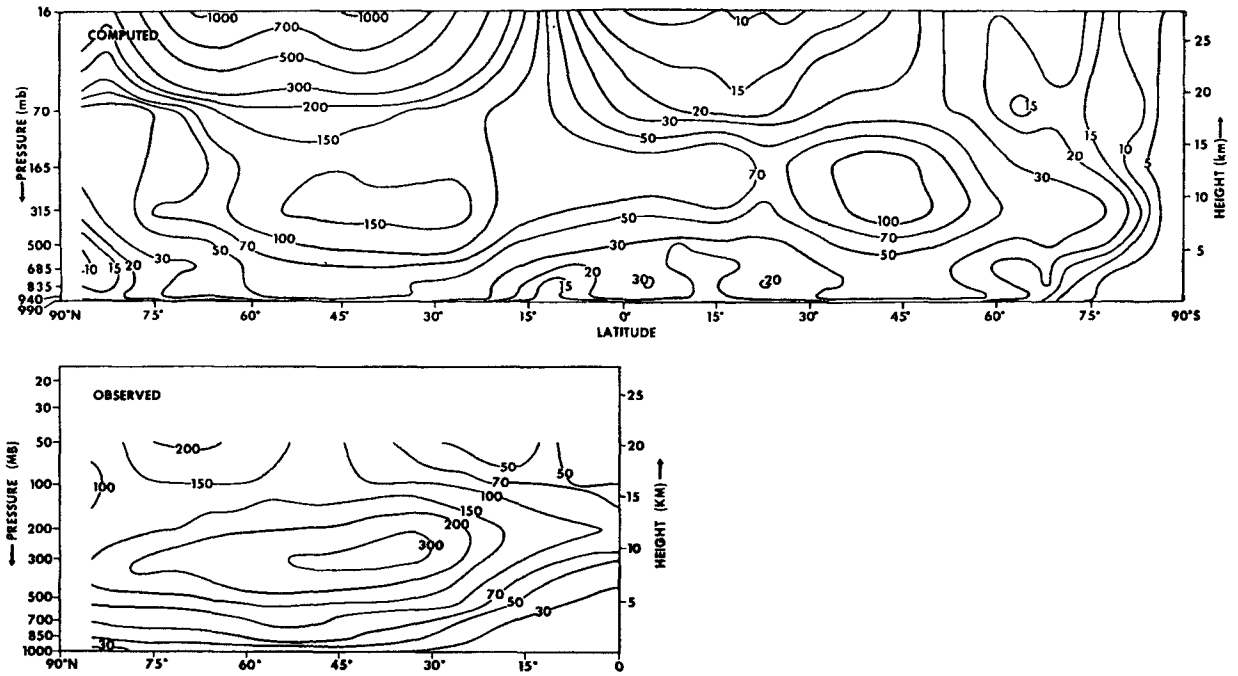

FIG. A3. Latitude-height distribution of eddy kinetic energy in the N48M atmosphere. Units are 10^{-3} J cm^{-2} mb^{-1}. The observed distribution was obtained by Oort and Rasmusson (1970b).

study and defined in Section 6, is slightly different from the definition adopted by Oort and Rasmusson. However, the two definitions may be regarded as similar to a first approximation.

According to this comparison, the distribution of eddy kinetic energy in the N48M model tropics is in reasonably good agreement with that in the actual tropics. The results described in Section 4 indicate that the eddy kinetic energy in the dry model tropics is much less than that in the moist. Therefore, it may be essential to have the effect of selective heating by condensation in order to have a realistic distribution of eddy kinetic energy in the model tropics.

Although the magnitude of eddy kinetic energy changes little in the model tropics resulting from the increase in the resolution of the horizontal finite differencing, it increases significantly in middle latitudes of the model. Because of this increase, the magnitude of the eddy kinetic energy of middle latitudes is more realistic in the N48M atmosphere than in the N24M.

In the polar regions, the magnitudes of the eddy kinetic energy is too small in the N48M as well as in the N24M atmosphere. This may be related to the excessive development of the polar high and the polar easterlies resulting from the perpetual duration of the insolation of January.

c. Eddy transport of angular momentum

Fig. A4 shows the latitude-height distribution of the northward transport of angular momentum by large-scale eddies in the N48M atmosphere. According to the comparison between this figure and Fig. 7.2, the northward eddy transport of angular momentum in the model

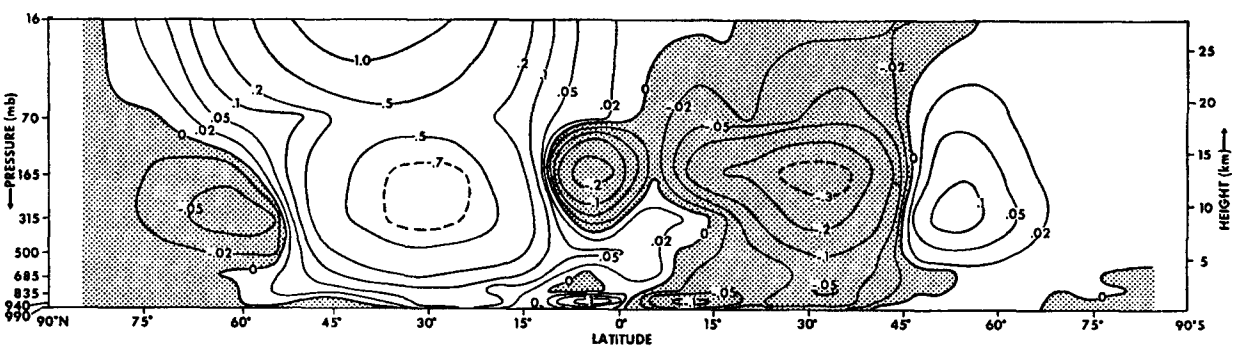

FIG. A4. Latitude-height distribution of the northward transport of absolute angular momentum by the large-scale eddies in the N48M atmosphere. Regions of southward transport are shaded. Units are 10^{29} gm cm^2 sec^{-1} day^{-1} mb^{-1}.

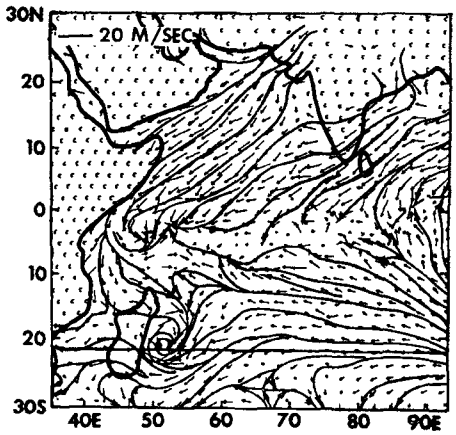

FIG. A5. Streamline map of winds at the 990-mb level of the N48M atmosphere on model day 26 in the Indian Ocean area. The heavy line through the vortex shows the location of the cross sections shown in Figs. A6 and A7. A letter "C" is plotted instead of a wind vector when the 990-mb level is below ground level.

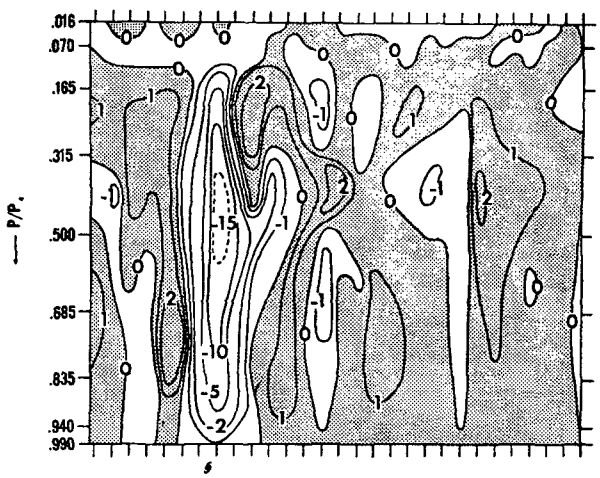

FIG. A7. Distribution of vertical p velocity (μb sec^{-1}) on day 26 along the cross section indicated by the solid line in Fig. A5.

subtropics increases significantly as a result of the increase in the resolution of the horizontal finite differencing and compares favorably with the eddy transport in the actual subtropics (see Fig. 7.1). The cross-equatorial transport of angular momentum, which is discussed in Section 7, is also evident in Fig. A4; its magnitude, however, is significantly less than the estimate obtained by Kidson *et al.* (1969) for the actual atmosphere.

d. Structure of the tropical cyclone

Examining the results of Section 5, which describes the structure of disturbances in the N24M model tropics, one gets the impression that the thermal structure and the field of upward motion around the center of a tropical cyclone is not resolved sufficiently by the finite difference grid system of the N24M model. In order to find out how they are resolved by the finer grid system of the N48M model, we analyzed a cyclone which developed in the western part of the Indian Ocean of the N48M model. Fig. A5 is the map of surface wind vectors on the 26th model day and shows a well-developed cyclone around 22.5S in the Indian Ocean. This cyclone is chosen for analysis because it is located at approximately the same place as the cyclone for which the cross-section analysis is made in Section 5. Figs. A6 and A7 show the cross sections of the temperature anomaly and the vertical p velocity of this cyclone. If one compares these cross sections with the corresponding ones in Figs. 5.9 and 5.7, one gets the impression that the structure of the cyclone in the N48M model is resolved better than that of the cyclone in the N24M model. (Note the pip marks at the bottom of the figures indicating grid points.) This comparison seems to suggest that the tropical cyclone in the model atmosphere is not a fictitious vortex produced by truncation error of the finite differencing but is a genuine consequence of the physical processes introduced into the model.

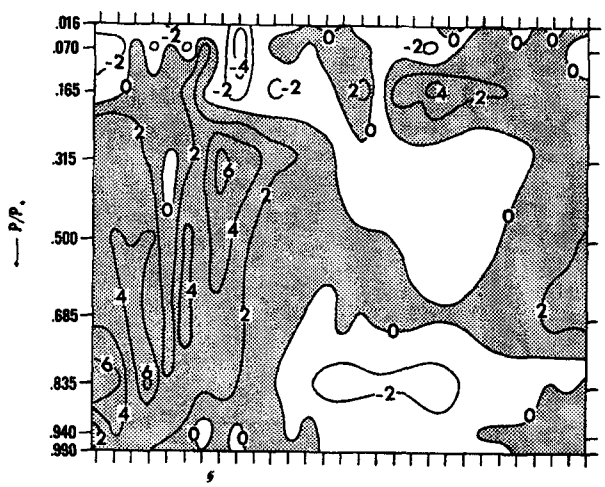

FIG. A6. Distribution of temperature deviation (°K) from the zonal mean on day 26 along the cross section indicated by the solid line in Fig. A5.

e. Very long waves in the model stratosphere

In the stratosphere of the model tropics, wave disturbances propagate with very long wavelengths. The left-hand side of Fig. A8 shows the time isopleths of the meridional component of the transient wind at the 70-mb level over the equator for a 53-day period of the time integration. (The transient wind vector is computed by subtracting the time mean wind vector from the total wind vector.) Careful inspection of this figure reveals the existence of long waves propagating westward. In order to identify these waves, we analyzed the meridional component of the wind into sinusoidal functions with respect to longitude. In the right-hand side of Fig. A8 time isopleths of the sum of wavenumbers 6, 7 and 8 are shown. This figure clearly indicates a

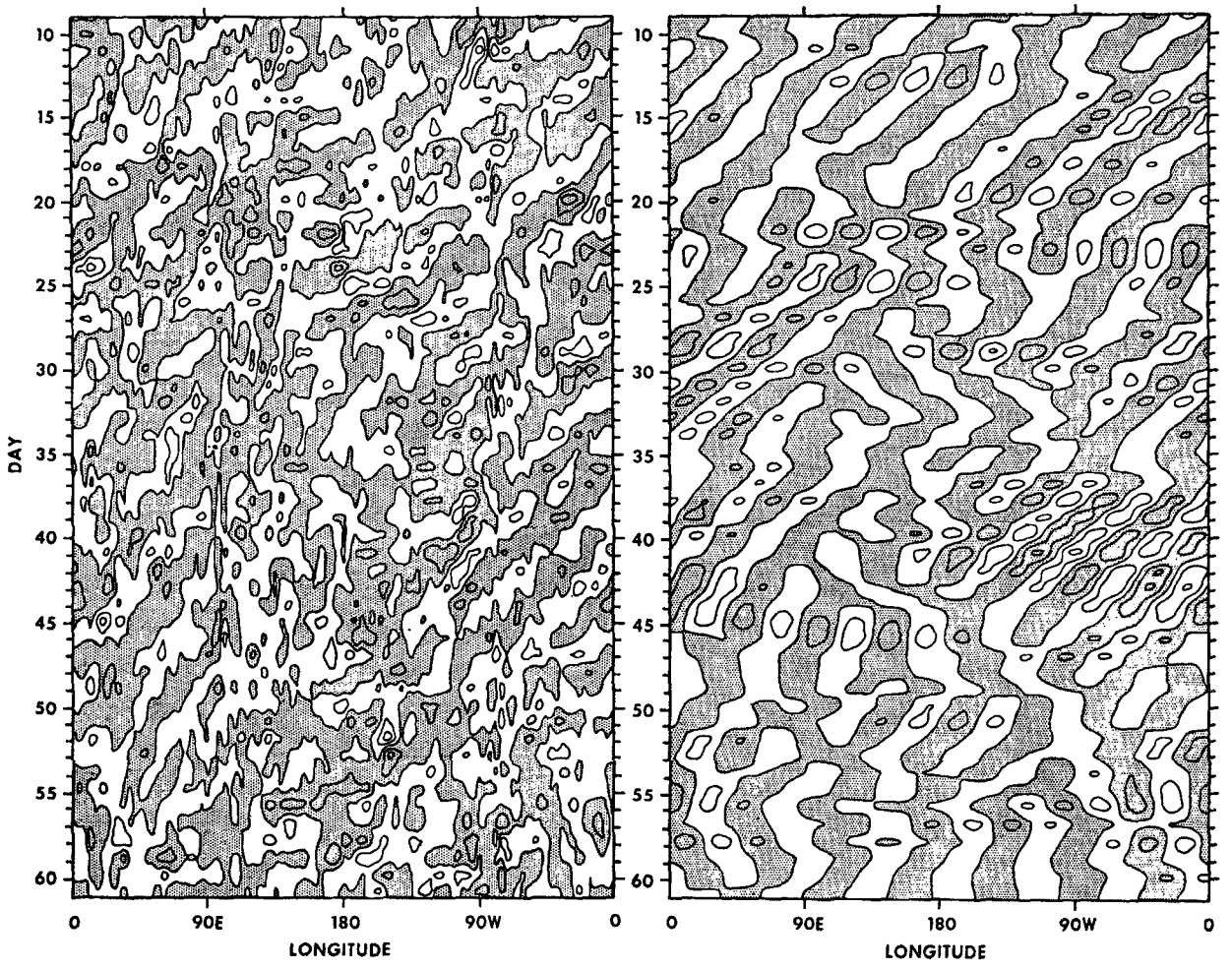

FIG. A8. Time isopleths of the meridional component of the transient wind at the 70-mb level over the equator. Left side of figure shows original data; negative areas are shaded and the contour interval is 5.0 m sec^{-1}. Right side of figure shows sum of wavenumbers 6, 7 and 8; negative areas are shaded and the contour interval is 2.0 m sec^{-1}.

westward propagation of waves with a phase velocity of approximately 13° longitude per day, a wavelength of 51° longitude, and a period of ~4 days. A westward propagation of a similar pattern in the time isopleths of the zonal component of the transient wind at the equator is not evident.

The features of this wave described above resemble those of the so-called "mixed Rossby-gravity wave" which was theoretically obtained by Matsuno (1966) and Rosenthal (1965) and discovered by Yanai and Maruyama (1966) in the actual tropical stratosphere. The Yanai-Maruyama wave, however, seems to have a somewhat longer wavelength and narrower latitudinal span than the wave in Fig. A8. Their wave is confined to the latitude belt ranging from approximately 12N to 12S, whereas the latitudinal span of the wave in the model stratosphere is somewhat wider. Nevertheless, it is interesting that the model is capable of producing waves which resemble waves found in the actual stratosphere.

In the middle stratosphere, i.e., at about the 16-mb level of the model, an ultra-long wave of a different kind propagates. The time isopleths of the zonal component of the transient wind, which is shown in the left-hand side of Fig. A9, reveal a rapid westward propagation of an ultra-long wave at the equator. This wave is more evident in the right-hand side of the figure, which shows the time isopleths of the sum of wavenumbers 2 and 3. This wave has a westward phase velocity of approximately 36° day^{-1}, a period of ~4 days and a wavelength of about 148° longitude. In the Southern Hemisphere, this wave is detectable up to 20S and has no phase shift with respect to latitude. However, the wave tilts from southwest to northeast in the Northern Hemisphere tropics and may contribute to the poleward transport of angular momentum there (see Fig. 7.3). The divergence of angular momentum caused by such transport may be partly responsible for the maintainance of the intense easterlies in the tropical stratosphere of the model.

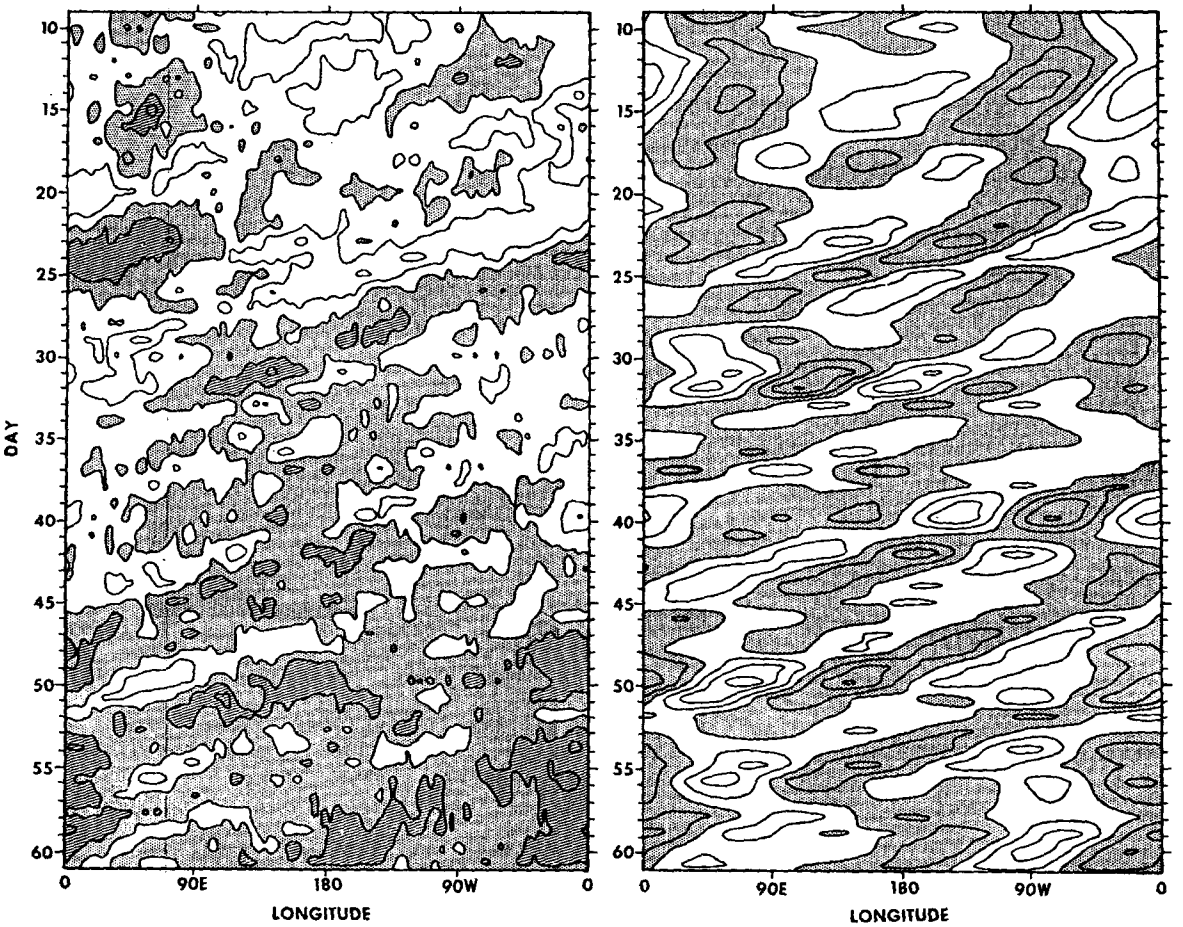

FIG. A9. Time isopleths of the zonal component of the transient wind at about the 16-mb level over the equator. Left side of the figure shows original data; negative areas are shaded (areas with easterly winds >5.0 m sec^{-1} have slant shading), and the contour interval is 5.0 m sec^{-1}. Right side of figure shows sum of wavenumbers 2 and 3; negative areas are shaded and the contour interval is 2.0 m sec^{-1}.

In this sub-section, we have shown that noteworthy very long waves propagate in the stratosphere of the model tropics. The spectra of eddy kinetic energy discussed in Section 4 reveal that very long waves also predominate in the troposphere of the model tropics. The structure of these long waves and the role of these waves in the general circulation of the model atmosphere will be the subject of a future study. Further increase in the resolution of the vertical finite differencing is required in order to represent the vertical structure of these equatorial waves with sufficient accuracy.

REFERENCES

Charney, J. G., 1969: A further note on large-scale motions in the tropics. *J. Atmos. Sci.*, **26**, 182–185.

Gray, W. M., 1968: Global view of the origin of tropical disturbances and storms. *Mon. Wea. Rev.*, **96**, 669–700.

Holloway, J. L., Jr., and S. Manabe, 1970: A global general circulation model with hydrology and mountains. Submitted to *Mon. Wea. Rev.*

Hydrographic Office, U. S. Navy, 1944. *World Atlas of Sea Surface Temperatures*, 2nd ed. H. O. Publ. No. 225.

——, 1969: *Monthly Charts of Mean, Minimum, and Maximum Sea Surface Temperature of the North Pacific Ocean.* Sp-123, 58 pp.

Johnson, D. H., 1969: The role of the tropics in the global circulation. *Proc. Joint Conf. Global Circulation of the Atmosphere*, London.

Kidson, J. W., D. G. Vincent and R. E. Newell, 1969: Observational studies of the general circulation of the tropics—long-term mean values. *Quart. J. Roy. Meter. Soc.*, **95**, 258–287.

Kurihara, Y., and J. L. Holloway Jr., 1967: Numerical integra- of a nine-level global primitive equations model formulated by the box method. *Mon. Wea. Rev.*, **95**, 509–530.

Mak, M. K., 1969: Laterally driven stochastic motions in the tropics. *J. Atmos. Sci.*, **26**, 41–64.

Manabe, S., 1969: Climate and ocean circulation. Part 1. The atmospheric circulation and the hydrology of the earth's surface. *Mon. Wea. Rev.*, **97**, 739–774.

——, and J. Smagorinsky, 1967: Simulated climatology of a general circulation model with a hydrologic cycle, II. Analysis of the tropical atmosphere. *Mon. Wea. Rev.*, **95**, 155–169.